Geochemistry and mineralogy of Neoproterozoic strata in northeastern Svalbard: re-evaluating the prevalence of basalt weathering during the early Neoproterozoic

Alexie E.G. Millikin[1*], Timothy M. Gibson[1,2], Justin V. Strauss[2], Kristin D. Bergmann[3], Nicholas J. Tosca[4], Ross P. Anderson[5,6], Galen P. Halverson[7], Tianran Zhang[2], and Alan D. Rooney[1]

[1]Department of Earth and Planetary Sciences, Yale University, New Haven, Connecticut 06511, USA

[2]Department of Earth Sciences, Dartmouth College, Hanover, New Hampshire 03755, USA

[3]Department of Earth, Atmospheric, and Planetary Sciences, Massachusetts Institute of Technology, Cambridge, Massachusetts 02139, USA

[4]Department of Earth Sciences, University of Cambridge, Cambridge CB2 3EQ, UK

[5]All Souls College, University of Oxford, Oxford OX1 4AL, UK

[6]Museum of Natural History, University of Oxford, Oxford OX1 3PW, UK

[7]Department of Earth and Planetary Sciences/Geotop, McGill University, Montreal, Quebec H3A 0E8, Canada

**Corresponding author email: Alexie.Millikin@Yale.edu*

ABSTRACT

Neoproterozoic strata of the Lomfjorden and lower Hinlopenstretet supergroups (early–middle Tonian Veteranen Group, middle–late Tonian Akademikerbreen Group, and the

Cryogenian–Ediacaran Polarisbreen Group) in northeastern Svalbard, Norway, represent one of the most complete and well-preserved terminal Proterozoic sedimentary successions worldwide. These strata have been used in numerous geochemical compilations to probe Neoproterozoic paleoenvironments, including patterns of global chemical weathering prior to the Snowball Earth events. Here, we present a new high-resolution geochemical dataset incorporating $\delta^{13}C$, $\delta^{18}O$ and $^{87}Sr/^{86}Sr$ data from carbonates with mineralogy, major and trace element and ε_{Nd} data from mudrocks to critically examine previously published datasets and better ally the succession with global Neoproterozoic records through a refined age model. We find that the geochemistry of Lomfjorden and lower Hinlopenstretet supergroup mudrocks is greatly affected by carbonate contamination and that rigorous filtering is imperative for extracting reliable provenance and weathering information. Previous studies ascribed relatively juvenile detrital Nd isotope signatures in these units to a mafic detrital source region in support of the hypothesis that basalt weathering contributed to global cooling during the Tonian prior to the Sturtian Snowball Earth event. In contrast, we present a new temporally extensive ε_{Nd} record that, when combined with elemental geochemical data, is best explained by the weathering of a combination of young and old granitic to granodioritic crustal sources, most likely sourced from the Grenville Province of Laurentia or Sveconorwegian Province of Scandinavia. Additionally, this new high-resolution mudrock dataset allows us to assess paleoenvironmental and weathering trends within the Lomfjorden and lower Hinlopenstretet supergroups, including the factors leading to exceptional fossil preservation in the ca. 790 Ma Algal Dolomite member of the Svanbergfjellet Formation, and post-Snowball Earth weathering dynamics.

INTRODUCTION

The Tonian Period (ca. 1000–720 Ma) was a dynamic interval of Earth history, recording changes in oceanic redox conditions, numerous biological innovations and paleogeographic reorganization associated with the formation and breakup of the supercontinent Rodinia (e.g., Li et al., 2008; Strauss et al., 2014; Cohen and Macdonald, 2015; Cole et al., 2016; Xiao and Tang, 2018). Tonian sedimentary successions also record the climatic descent into the Cryogenian (720–635 Ma) Snowball Earth events and are key to understanding boundary conditions that made Earth susceptible to such drastic cooling.

The initial rifting of Rodinia (ca. 825 Ma; Li et al., 2008), was accompanied by the emplacement of voluminous mafic large igneous provinces (LIPs) at low latitudes, likely leading to relatively high chemical weathering rates (Ernst et al., 2008; Cox et al., 2016b; Ernst and Youbi, 2017) given that basaltic material weathers faster than felsic material under the same climatic conditions (e.g., Dessert et al., 2001; Ibarra et al., 2016). The increased flux of cations from LIP weathering and attendant aqueous carbonate formation has the potential to drive cooling. The "Fire and Ice" hypothesis posits that enhanced global silicate weathering lowered CO_2 to a level at which the ice-albedo feedback would push Earth into a global glaciation (Goddéris et al., 2003; Donnadieu et al., 2004). As such, LIP weathering has been implicated in contributing to the onset of the first Cryogenian Snowball Earth event: the Sturtian glaciation (Cox et al., 2016b). The most precise dates for glacial initiation, between 717.4 ± 0.1 Ma and 716.9 ± 0.2 Ma (Macdonald et al., 2010 and 2018), follow emplacement of the Franklin LIP (719.86 ± 0.21 Ma and 718.61 ± 0.30 Ma; Pu et al., 2022; Dufour et al., 2023) by 0.9 to 1.6 Ma, a viable duration for the drawdown of CO_2 via silicate weathering (Macdonald and Swanson-Hysell, 2023). In addition to immediately pre-Sturtian cooling, long-term weathering of several large flood basalt provinces emplaced during the Tonian has been suggested to increase Earth's susceptibility to Snowball glaciation (e.g., Cox et al., 2016b; Zhou et al., 2020).

Weathering of continental flood basalts should impart a distinct elemental and isotopic signature on the sedimentary record. Marine Os and Sr isotope data, which reflect globally integrated weathering fluxes, become less radiogenic from the middle to late Tonian (Cox et al., 2016b; Zhou et al., 2020; Park et al., 2020; Chen et al., 2022), suggesting an increased flux of these elements from mafic sources. However, this record could also be interpreted to reflect juvenile arc weathering (Park et al., 2020). Relatively juvenile (high) Nd isotope values of middle to late Tonian sedimentary successions have been attributed to large detrital fluxes of mafic LIP material (Barovich and Foden, 2000; Wang et al., 2011; Cox et al., 2016b); however, only some of these studies presented accompanying major and trace element data to differentiate between juvenile mafic and felsic sources, critical to resolving the relative influence of LIP and arc weathering on climate in the Tonian.

The Lomfjorden and lower Hinlopenstretet supergroups represent one of the most complete and well-preserved Neoproterozoic successions worldwide (Halverson et al., 2018a, 2018b). This succession has yielded profound insights into Neoproterozoic paleontology (e.g., Knoll, 1982; Knoll et al., 1991; Butterfield et al., 1994; Mughal et al., 2025), biogeochemical cycles (Maliva et al., 2005; Maloof et al., 2006; Halverson et al., 2007a, 2007b; Tosca et al., 2010, 2011; Chakrabarti et al., 2012; Kunzmann et al., 2015; Lu et al., 2017; Wörndle et al., 2019; Roest-Ellis et al., 2023), and climate (e.g., Fairchild et al., 1989, 2016; Fairchild and Spiro, 1990; Halverson et al., 2004; Bao et al., 2009; Hoffman et al., 2012). Building upon recent advances in geochronology and basin subsidence age-depth modelling (Figure 1A; Halverson et al., 2022; Millikin et al., 2022; Zhang et al., 2023), we generate a new composite and age-calibrated stratigraphic section for the

Lomfjorden and lower Hinlopenstretet supergroups of northeastern Svalbard (over 6 km of stratigraphic thickness) and couple it with new high-resolution mineralogy, bulk-rock elemental chemistry, carbonate $\delta^{13}C$, $\delta^{18}O$, and $^{87}Sr/^{86}Sr$ chemostratigraphy, and mudrock detrital Nd isotope chemostratigraphy. This dataset allows us to explore the extent of LIP weathering in the Tonian and further probe local Neoproterozoic weathering conditions in northeastern Svalbard, as well as provide new insight into the influence of weathering on exceptional fossil preservation in the Svanbergfjellet Formation.

GEOLOGIC BACKGROUND

The Svalbard archipelago, located north of Norway on the Barents Shelf, consists of three distinct litho-tectonic provinces that were amalgamated during the Silurian–Devonian Caledonian Orogeny. The Southwestern, Northwestern, and Eastern provinces are separated by north-south-oriented strike-slip faults (Figure 1B). The Eastern province comprises Ny Friesland, the eastern part of Spitsbergen, and the island of Nordaustlandet, and is divided into two basement domains: the West Ny Friesland and Nordaustlandet terranes, which are separated by the Eolussletta Shear Zone (ESZ, also called the Veteranen Line; Figure 1B). The Nordaustlandet terrane comprises units on both sides of Hinlopenstretet, in both eastern Ny Friesland and Nordaustlandet, which are the subject of this study.

Neoproterozoic strata in eastern Ny Friesland comprise the Veteranen and Akademikerbreen groups, together forming the Lomfjorden Supergroup, and the Polarisbreen and Oslobreen groups, forming the Hinlopenstretet Supergroup (Figure 1B; Dallmann, 2015). The Lomfjorden and Hinlopenstretet supergroups are analogous to the Hecla Hoek Succession as used in Halverson et al. (2018a), Gibson et al. (2021), Millikin et al. (2022), and Zhang et al. (2023), but we refrain from using this terminology as it was originally defined to include underlying metasedimentary and igneous units on Ny Friesland (Dallmann, 2015). Stratigraphic units from eastern Ny Friesland are well correlated with units found in northeastern Nordaustlandet (Harland and Wilson, 1956; Sandelin et al., 2001); thus, following recent work by Halverson et al. (2018a) and Gibson et al. (2021), we adopt the stratigraphic nomenclature of Ny Friesland to refer to units on both sides of Hinlopenstretet (Figure 1B).

In eastern Ny Friesland, the base of the Veteranen Group and its contact with underlying basement units is not exposed. In Nordaustlandet, the Galtedalen Group unconformably overlies both the late Mesoproterozoic metasedimentary Brennevinsfjorden Group and early Tonian igneous Kapp Hansteen Group, with angular unconformities separating all three units (Gee et al., 1995; Johansson et al., 2005). The lowermost Galtedalen Group is only preserved and exposed in sporadic outcrops across northern Nordaustlandet (Sandelin et al., 2001). The remaining strata of the Veteranen, Akademikerbreen, Polarisbreen and Oslobreen groups crop out continuously across eastern Ny Friesland and northern Nordaustlandet (Figure 1B).

Underlying units provide a maximum age for the Galtedalen Group. The maximum depositional age of the Brennevinsfjorden Group is ca. 1050 Ma, based on the youngest detrital zircon U–Pb age reported in Lorenz et al. (2012) and reported ages from the Kapp Hansteen Group and other associated igneous and metamorphic rocks are ca. 970–940 Ma (Figure 1A; Gee et al., 1995; Johansson et al., 1999). Volcanic rocks of the Kapp Hansteen Group are interpreted to have formed in a collisional or arc setting based on their peraluminous compositions, the abundance of inherited Mesoproterozoic zircon grains, and Nd isotopic signatures (Johansson et al., 1999).

The Veteranen Group comprises ~4.4 km of mixed carbonate and siliciclastic strata (Wilson, 1958) and is subdivided into four conformable formations, the Kortbreen, Kingbreen, Glasgowbreen, and Oxfordbreen formations (Figure 1A; Harland et al., 1966). Despite these strata yielding well-preserved early Neoproterozoic microfossil populations (Knoll, 1982; Knoll and Swett, 1985), Gibson et al. (2021) was the first investigation to provide a detailed sedimentological framework, and to date no detailed geochemical or geochronologic work has been done on these units. The depositional age of the basal Veteranen Group is only constrained by a zircon U–Pb maximum depositional age of 879.9 ± 1.1 Ma from the Bogen Member of the Kingbreen Formation (Zhang et al., 2023). The Veteranen Group records nearshore marine to potentially terrestrial sedimentary environments influenced by tide and storm sedimentation (Gibson et al., 2021). Although no major unconformities are recognized within the Veteranen Group, evidence for subaerial exposure occurs throughout the succession indicating depositional hiatuses. Calcareous intervals within the Veteranen Group represent short-lived windows of diminished terrigenous input (Gibson et al., 2021).

Carbonate content gradually increases in the uppermost Veteranen Group, which transitions into a thick carbonate platform within the overlying Akademikerbreen Group (Halverson et al., 2018a). Coupled Bayesian inference and thermal subsidence modelling provides an estimated age of 840.4 $^{+}$18.6/$^{-}$23.6 Ma for the Veteranen-Akademikerbreen contact (Zhang et al., 2023). The ~2-km-thick Akademikerbreen Group is separated into the Grusdievbreen, Svanbergfjellet, Draken, and Backlundtoppen formations (Figure 1A; Wilson, 1961). Only two minor disconformities are recognized within the Akademikerbreen Group, the first separates the informal lower and upper Grusdievbreen members and the second is the contact between the Lower Dolomite and Lower Limestone members of the Svanbergfjellet Formation (Halverson et al., 2018a). Providing a robust correlation tie-point and minimum age constraint for the Veteranen Group, the ca. 810 Ma Bitter Springs carbon isotope excursion (CIE) is recorded in the upper Grusdievbreen and lower

Svanbergfjellet formations (Halverson et al., 2007b, 2018a, 2018b; Macdonald et al., 2010; Swanson-Hysell et al., 2015). A Re–Os age of 791.1 ± 4.9 Ma from the top of the Lower Limestone member of the Svanbergfjellet Formation is consistent with this correlation (Zhang et al., 2023). Bayesian age-depth modelling of the Akademikerbreen Group provides ages of 784 $^{+}7.4/^{-}10.9$ for the Svanbergfjellet-Draken contact and 739.1 $^{+}9.5/^{-}9.7$ Ma for the Backlundtoppen Formation-Polarisbreen Group contact, which are consistent with carbonate carbon isotope correlated ages (Halverson et al., 2022; Zhang et al., 2023).

The Akademikerbreen-Polarisbreen transition is marked by a silicified solution breccia in Ny Friesland, suggesting subaerial exposure, but the contact appears transitional in Nordaustlandet (Halverson et al., 2018a). The Polarisbreen Group comprises the Elbobreen, Wilsonbreen and Dracoisen formations (Figure 1A). A Re–Os age of 737.5 ± 9.6 Ma from the Russøya Member in the basal Elbobreen Formation (Millikin et al., 2022) confirms correlation of a negative CIE within the Russøya Member to pre-Sturtian ca. 735 Ma CIEs in Northwest Canada and Ethiopia (Rooney et al., 2014; Strauss et al., 2014; MacLennan et al., 2018). This correlation, along with variable truncation of the CIE, suggest that a significant erosional unconformity separates the Russøya Member from the overlying Petrovbreen diamictite (Halverson et al., 2018a; Millikin et al., 2022). The Petrovbreen Member consists of a thick-bedded and massive glaciomarine diamictite and is correlated globally with ca. 717–660 Ma Sturtian glacial deposits.

The Petrovbreen Member is overlain by dolomitic shales and siltstones of the Macdonaldryggen Member and carbonates of the Slangen Member, recording mid-Cryogenian non-glacial deposition (Fairchild et al., 2016). The Slangen Member is transitional with aeolian quartz arenites of the Bråvika Member (basal Wilsonbreen Formation) where it is present (Reahl et al., 2021), and in other locations the contact between the Slangen Member and glaciogenic strata of the Wilsonbreen Formation is sharp and silicified. The Wilsonbreen Formation is correlated globally with ca. 645−635 Ma Marinoan glacial strata based on the presence of a typical Marinoan cap dolostone and a Re–Os age of 631.2 ± 3.8 Ma in the conformably overlying Dracoisen Formation (Halverson et al., 2004; Millikin et al., 2022).

METHODS

Field Sampling and analytical methods

Mudrock and carbonate samples for geochemical and mineralogical analysis were collected over field seasons from 2016–2019 from the Lomfjorden and lower Hinlopenstretet supergroups and underlying Brennevinsfjorden and Kapp Hansteen groups. All samples were collected within the context of measured stratigraphic sections (see Table DR1 for coordinates). A summary of the various methodologies is provided below and detailed descriptions of all analytical methodologies and data processing approaches can be found in the Supplementary Material[1].

Mudrock and igneous samples were cut and polished to remove weathered edges and crushed to a fine (~30 μm) powder using either a zirconium or ceramic grinding container and puck. Carbonate hand samples were cut perpendicular to bedding and then micro-drilled parallel to lamination, avoiding visible veins, cements, fractures, or any siliciclastic components. 403 mudrock and 272 carbonate samples were analyzed for major and trace element chemistry at Activation Laboratories Ltd. in Ancaster, Ontario, Canada (Table DR2).

Aliquots of a subset of powdered mudrock samples (n = 208) were analyzed for mineralogy via X-ray diffraction on a Panalytical Empyrean X-ray diffractometer at the University of Oxford (operated at 40kV and 40mA with a Co-Kα source), including semi-quantitative bulk mineralogy determined using the reference intensity ratio method from data acquired across the 5−80° 2θ range. Group-level clay mineral identification and relative abundance were determined using data acquired from randomly oriented powders across the 69–75° 2θ area (Figure DR1; Table DR3; Anderson et al., 2018).

A subset of powdered mudrock samples (n = 106) and four samples from the Kapp Hansteen Group were analyzed for Sm–Nd isotopes in the Yale Metal Geochronology and Geochemistry Center. Sample powders were ignited to remove organic material, spiked with an isotopically enriched ^{150}Nd-^{149}Sm tracer and digested using Aqua Regia and a combination of nitric and hydrofluoric acids. Nd and Sm were isolated through three-stage gravity and vacuum driven column chromatography based on procedures from Pin and Zalduegui (1997) and Yang et al. (2010). The separates were analyzed via multi-collector inductively coupled plasma mass spectrometery (MC-ICP-MS) on a Thermo Scientific Neptune. Sm and Nd concentrations and ^{147}Sm/^{144}Nd for each sample were calculated using measured isotopic ratios and sample and spike mass. Sample ^{143}Nd/^{144}Nd and ^{147}Sm/^{144}Nd ratios were combined with a simplistic age model (described below) to calculate ε_{Nd} at the time of sedimentation ($\varepsilon_{Nd(T)}$ where T represents depositional age). For this calculation, the chondritic (CHUR) reference values used were ^{143}Nd/^{144}Nd = 0.512638 and ^{147}Sm/^{144}Nd = 0.1966, and the decay constant for ^{147}Sm to ^{143}Nd was assumed to be 6.54×10^{-12} a^{-1} (Table DR4; Goldstein et al., 1984).

A subset of carbonate samples (n = 119) was analyzed for Sr isotopes at the Yale Metal Geochronology and Geochemistry Center. Sample powders were leached sequentially following protocols of Bailey et al. (2000) and Bellefroid et al. (2018). Aliquots of each sample leachate were analyzed on a Thermo Scientific iCAP Q ICP-MS to determine elemental abundances (Ca, Mg, Sr, Fe, Mn, and Rb) and assess which leachate comprises the most primary, seawater-derived carbonate phase. For each sample the leachate with the highest Sr concentration and lowest Mg/Ca, Mn/Sr, Fe/Sr, and Rb/Ca was selected for Sr isotope analysis on the Neptune MC-ICP-MS (Figures DR2 & 3; Table DR5).

A set of carbonate samples (*n* = 1784) was analyzed for carbonate $\delta^{13}C$ and $\delta^{18}O$ isotopes at Massachusetts Institute of Technology (MIT) following the procedures outlined in N. Anderson et al. (2021). Carbonate samples were drilled to avoid fracturing and veining using a carbide bit. Powders weighing ~50–100 µg were heated to remove residual water and volatiles. Samples were then reacted with 150 µL of H_3PO_4 and the resultant CO_2 gas was measured using a Nu Carb automated sample preparation unit held at 70°C and $\delta^{13}C$ and $\delta^{18}O$ were measured simultaneously on a Nu Perspective isotope ratio mass spectrometer. Data were processed using the "D47crunch" Python package (Daëron, 2023) and are reported as per mil difference from Vienna Pee Dee Belemnite in Table DR6. The long-term average external repeatability (1 standard deviation) for standards is 0.06‰ for $\delta^{13}C$ and 0.25‰ for $\delta^{18}O$. The complete dataset, including metadata, measurement parameters, standard data and raw sample data can be found at https://doi.org/10.5281/zenodo.14276719 (Bergmann et al., 2024).

Construction of composite stratigraphic section and age model

For plotting geochemical data, we constructed a composite stratigraphic section for the Lomfjorden and lower Hinlopenstretet supergroups based on detailed stratigraphic logs and $\delta^{13}C$ and $\delta^{18}O$ chemostratigraphy (Figure DR4). Due to the sparse and discontinuous nature of outcrop from the Galtedalen Group, the 0 m datum of the composite is the type-section (T1831) of the Veteranen Group at Faksevågen, Ny-Friesland (location 1 on Figure 1B) from Gibson et al. (2021). The composite section continues through the Akademikerbreen Group at nearby De Geerbukta and Lomfjorden (locations 2 & 3 on Figure 1B), and at Murchisonfjorden in eastern Nordaustlandet (location 4 on Figure 1B) for the uppermost Akademikerbreen Group and Russøya Member of the Polarisbreen Group. Stratigraphic sections were not measured through Cryogenian glacial strata in this study, so thicknesses of those units were estimated based on literature sources (Fairchild et al., 2016; Halverson et al., 2018a, 2018b). Stratigraphic sections from the mid-Cryogenian Macdonaldryggen Member and post-Marinoan Dracoisen Formation of the Polarisbreen Group from Buldrevågen and Murchisonfjorden were correlated to the composite section (locations 3 & 6 on Figure 1B). Samples from additional sections in this study were correlated to the composite section based on regional field relationships. Geochemical and Nd isotope data, including 80 mudrock and three diamictite samples, from Kunzmann et al. (2015) and Cox et al. (2016b) from the Lomfjorden and lower Hinlopenstretet supergroups and their proposed counterparts from East Greenland have also been integrated into our composite stratigraphic framework.

For the purposes of plotting geochemical data temporally and calculating their associated $\varepsilon_{Nd(T)}$ values, we have constructed an age model for the Lomfjorden and lower Hinlopenstretet supergroups based on linear interpolation for the Veteranen Group, thermal subsidence age-depth modeling for the Akademikerbreen and lower Polarisbreen groups, and existing geochronology and global correlations for the remainder of the Polarisbreen Group (Millikin et al., 2022; Zhang et al., 2023). Details about the composite section and age model can be found in the Supplementary Material, Figure DR4 and Table DR7.

RESULTS

Mudrock geochemical subsets and data filtering

Mudrock samples were filtered based on their carbonate content using Ca/Al ratios (molar proportion) given a clear correlation between Ca/Al and carbonate content, Al_2O_3 and CaO

(Figures 2 & DR5). Of the 483 mudrocks from the Lomfjorden and lower Hinlopenstretet supergroups and Brennevinsfjorden Group analyzed in this study and compiled from Kunzmann et al. (2015), 93 have been filtered into a “Ca/Al > 1” subset and 80 into a “Ca/Al 0.3−1” subset (Figure DR6; Tables 1 & DR2). Six samples from Kunzmann et al. (2015) and two from this study did not have enough information to filter via these criteria and were included in their own “no filter data” subset. Four samples with fluorapatite and middle rare earth element (MREE) enrichments and 11 samples characterized by MREE depletion have been filtered into additional “Fluorapatite” and “MREE Depleted” subsets, respectively, to isolate samples that have been affected by heavy mineral sorting (Figure 3). Finally, 287 samples comprise the “Low Ca/Al” subset of siliciclastic mudrocks with Ca/Al < 0.3 that were not included in the “MREE Depleted” or “Fluorapatite” subsets. See the Supplementary Material for further discussion of these subsets.

Mudrocks within the “Ca/Al > 1” and “Ca/Al 0.3−1” subsets have distinct major oxide chemistry and trace element concentrations, and to some extent trace element ratios, when compared with samples with Ca/Al < 0.3 (Figures 3, 4, & 5). Although REE concentrations and ratios in the “Fluorapatite” and “MREE Depleted” profiles are distinct from the “Low Ca/Al” samples, they are indistinguishable in other trace element ratios and major element chemistry. As such, samples from the “Low Ca/Al”, “MREE Depleted”, and “Fluorapatite” subsets are primarily used to assess trends in provenance and weathering throughout the Lomfjorden and lower Hinlopenstretet supergroups and are collectively referred to as the “provenance and weathering subset” (Table 1).

Geochemical and mineralogical characterization of provenance and weathering subset

Major oxide chemistry

Samples within the "provenance and weathering subset" typically have 58.8–65.5% SiO_2, 14.0–18.4% Al_2O_3, 3.6–5.0% K_2O, 3.3–6.0% Fe_2O_3, 1.4–2.7% MgO, and 0.2–1.2% CaO with minor MnO, Na_2O, TiO_2, and P_2O_5 (all ranges quoted as inner quartile range (IQR)). Sample loss on ignition measurements were typically 3.7–7.2%. Within this subset of mudrocks there are moderate positive correlations between Al_2O_3 and K_2O (r^2=0.6), Al_2O_3 and TiO_2 (r^2=0.5), MgO and Fe_2O_3 (r^2=0.4), and MgO and CaO (r^2=0.5; Table DR2, Figure DR7).

Major oxide molar proportions are displayed on ternary ACNK (Al_2O_3−CaO^*+Na_2O−K_2O) and ACNKFM (Al_2O_3−CaO^*+Na_2O+K_2O−FeO_T+MgO) diagrams (Figure 6), which are utilized to investigate provenance, weathering, diagenesis and sorting in sedimentary units. The vertical axis on the ACNK ternary is also equivalent to the Chemical Index of Alteration (CIA; Nesbitt and Young, 1982, 1989). Samples from most units of the Lomfjorden and lower Hinlopenstretet supergroups, including all formations of the Veteranen Group, plot consistently with each other on the ACNK and ACKFM diagrams. Samples from the Dracoisen Formation are distinguished by a lower molar proportion of Al_2O_3 than the rest of the strata and mudrocks from the Russøya Member of the Elbobreen Formation and Algal Dolomite member of the Svanbergfjellet Formation typically have the highest molar proportion of Al_2O_3 and CIA (see Figure 7 for stratigraphic context). In contrast, mudrocks from the Arena Formation, the mid-Cryogenian non-glacial unit from East Greenland, are geochemically distinct from the rest of the samples in the "provenance and weathering subset". These mudrocks are characterized by a low molar proportion of K_2O and plot closer to the FeO_T+MgO apex on the ACNKFM diagram (Figure 6B). Mudrock samples with Ca/Al > 0.3 plot more consistently with carbonate samples than mudrocks, that is, closer to the CaO^*+Na_2O apex on the ACNK diagram and the FeO_T+MgO apex on the ACKFM ternary (Figure 6).

Mineralogy

Samples within the "provenance and weathering subset" are typically composed of 25.7–56.6% quartz, 0.0–17.0% feldspar (both plagioclase and K-feldspar), minor carbonate and accessory minerals, and 32.0–63.4% clay minerals (all ranges quoted as IQR as percent of whole rock; Table DR3). The most abundant clay minerals are montmorillonite, muscovite, and illite, which cannot be differentiated using the methodology of this study and will collectively be referred to as "MMI". Other common clay minerals are Fe chlorite, berthierine, Mg chlorite, smectite, and kaolinite. The abundance of clays and dominant clay mineralogy (MMI) remains roughly constant throughout most of the Lomfjorden and lower Hinlopenstretet supergroups, except for in the Svanbergfjellet Formation (Figure 8), which is the only unit with significant kaolinite as seen in samples from both Lomfjorden and De Geerbukta.

Trace element chemistry

Immobile trace element ratios are relatively homogenous in mudrocks of the Lomfjorden and lower Hinlopenstretet supergroups. REE concentrations normalized to chondritic values show a pattern similar to post-Archean Australian Average Shale (PAAS) with enrichment in the light REEs (LREE; ~100× chondrite) compared to heavy REE (HREE; ~10-15× chondrite), a flat HREE slope, and Eu anomalies (Figure 3; McLennan, 1989).

Within the "provenance and weathering subset" the range of Th/Sc ratios is 0.59 to 1.71, excluding outliers (defined as 1.5×IQR), and is roughly normally distributed about a mean of 1.15, with 75% of the data falling above 1. Eu anomalies are also normally distributed about a mean of 0.59, with a range of 0.5 to 0.7 excluding outliers (Figure 9). The five samples from the Arena Formation originally published in Kunzmann et al. (2015) and a few samples from the Russøya Member of the Elbobreen Formation have low Th/Sc (~0.3–0.5), accompanied by high concentrations of Sc and MgO (Table DR2) in most samples. Ti/Al ratios show minimal variation throughout the Lomfjorden and lower Hinlopenstretet supergroup mudrocks and are similar to PAAS and average upper continental crust (UCC; Figure DR8). Only samples from the Arena Formation have consistently high Ti/Al, although individual samples from other units, including one from the Russøya Member, have high Ti/Al. Many samples from the Algal Dolomite member of the Svanbergfjellet Formation have low Ti/Al.

Within the "provenance and weathering subset", Zr/Sc has an IQR of 13.2 to 38.6 (excluding outliers) but the distribution is skewed towards higher values with many outliers that reach up to 103. These samples span the entire stratigraphic range. Elevated Zr/Sc values plot on a trend characteristic of sedimentary recycling—however it is notable that Zr/Sc does not correlate with CIA—or a zircon-rich source region (Figures DR9 & 10; McLennan et al., 1993). On discrimination diagrams typically used to investigate sediment source and tectonic setting (Figure 10), mudrocks from the Lomfjorden and lower Hinlopenstretet supergroups typically plot within the continental arc setting with some samples, especially from the Veteranen Group, in the passive margin field, characterized by high Zr and Hf. Samples from the Svanbergfjellet Formation span a wide range in Zr concentrations, and many samples from the Algal Dolomite member are depleted compared to the other mudrocks.

Nd isotopes

The detrital Nd isotope signatures ($\varepsilon_{Nd(T)}$) recorded in mudrocks of the Lomfjorden and lower Hinlopenstretet supergroups range from -12.3 to -1.3 (n = 135; Figure 7; Table DR4). For reference, juvenile mid-ocean ridge basalt (MORB) is estimated to have a $\varepsilon_{Nd(T)}$ of about +8 at 800 Ma (Shirey et al., 2008), and evolved upper continental crust typically has $\varepsilon_{Nd(T)} < -10$ (McLennan et al., 1993). The fractional deviation of the sample $^{147}Sm/^{144}Nd$ ratio from a chondritic reservoir, a compositional metric, f_{SmNd}, ranges from -0.27 to -0.62, with one outlier at -0.09. $\varepsilon_{Nd(T)}$ values from most stratigraphic units sampled span a relatively narrow range (< 4 ε units) and are consistent between this study and previously published results (Cox et al., 2016b). Mudrock Nd isotope data do not correlate with Ca/Al (Figure 11); thus all data, regardless of subset, are considered in the discussion below.

Samples from the Galtedalen Group define a narrow $\varepsilon_{Nd(T)}$ range from -5 to -5.2 (n = 3), while those from the Veteranen Group range from -2.6 to -6.4 (n = 54). Formational averages are between -4 and -5 and are indistinguishable from each other (Figures 9 & 11). One sample from the lower Grusdievbreen Formation has the highest $\varepsilon_{Nd(T)}$ measured (-1) and is more juvenile than the two samples from the upper Grusdievbreen, for which $\varepsilon_{Nd(T)}$ is between -4.1 and -4.3, consistent with the Galtedalen and Veteranen groups. Samples from the Svanbergfjellet Formation are defined by more evolved (lower) $\varepsilon_{Nd(T)}$, ranging from -5.1 to -8.6 (with one outlier at -10.9) and an average of -7.2 (n = 33). $\varepsilon_{Nd(T)}$ values increase slightly in the Draken Formation, ranging from -4.9 to -7.9 with an average of -5.9 (n = 5). A single sample from the lower Backlundtoppen records an $\varepsilon_{Nd(T)}$ of -5.5. Samples from the Kinnvika Member of the Backlundtoppen Formation are some of the most juvenile within the Lomfjorden and lower Hinlopenstretet supergroups, ranging from -2.6 to -5.5 with an average of -3.3 (n = 5). $\varepsilon_{Nd(T)}$ for Russøya Member samples span a wide range from -

1.8 to -8.4 (n = 12). While most of the samples have $\varepsilon_{Nd(T)}$ between -4.5 and -6.4, three samples are even more juvenile than the Kinnvika Member, including the two stratigraphically highest samples.

The most significant change in Nd isotope values throughout the Lomfjorden and lower Hinlopenstretet supergroups begins with the mid-Cryogenian Macdonaldryggen Member, which preserves a much more evolved $\varepsilon_{Nd(T)}$ signature with an average of -9.6 (n = 12) and range of -6.3 to -12.2. Diamictite samples from the Wilsonbreen Formation are all from Cox et al. (2016b) and do not have any accompanying major element geochemical data to apply similar filters. $\varepsilon_{Nd(T)}$ values for the Wilsonbreen Formation all fall between -8 and -8.6 with an average of -8.3 (n = 3). The Dracoisen Formation is defined by $\varepsilon_{Nd(T)}$ values ranging from -10.3 to -11.3 with an average of -10.9 (n = 14).

The Nd isotopic signatures of the Nordaustlandet Terrane basement units define a narrow range that overlaps with the more juvenile values from the mudrocks (Figure 11). The sample analyzed from the metasedimentary Brennevinsfjorden Group has $\varepsilon_{Nd(T)}$ of -3, and the $\varepsilon_{Nd(T)}$ of the four Kapp Hansteen Group samples ranges from -2.4 to -3.6, consistent with previous analyses on the Kapp Hansteen andesites and quartz porphyries ranging from -2.2 to -3.3 (Johansson et al., 1999).

Sr isotopes

Sr isotope ($^{87}Sr/^{86}Sr$) values from carbonates of the Lomfjorden and lower Hinlopenstretet supergroups range from 0.706009 to 0.718784 (Table DR5). While data from this study span a much larger isotopic range than values for the Akademikerbreen and Polarisbreen groups reported by Halverson et al. (2007a) and Cox et al. (2016b), this is an artifact of analytical protocol (Figure 12). Following convention, both previous studies measured Sr isotopes on only the least altered samples. Here Sr isotopes were measured instead on a series of sequential leachates on unfiltered samples in an aim to extract primary seawater $^{87}Sr/^{86}Sr$ data even from altered or contaminated samples. Despite the success of this approach in other locations (Bellefroid et al., 2018), about half of the samples in this study yielded Sr isotope data that are significantly higher than reasonable seawater values for the Neoproterozoic (>0.709; Figure DR3F; Chen et al., 2022).

We present all Sr isotope data in Table DR5 and filter samples using a whole rock Sr concentration cut-off of >500 ppm, which has been used previously for this succession (Halverson et al., 2007a). The resulting dataset largely agrees with values from Halverson et al. (2007a) and Cox et al. (2016b) but does not exclude many data points with elevated $^{87}Sr/^{86}Sr$, which is consistent with other work done on these strata (Fairchild et al., 2016). After this first filter, no correlations between $^{87}Sr/^{86}Sr$ and whole rock geochemical data typically used as additional filters were evident (e.g., Mn/Sr, Fe/Sr, Rb/Sr), even within individual stratigraphic units (Figure DR3). However, we do impose an additional filter using the Sr concentration in the leachate analyzed of >0.5 ppm. This final filtered dataset includes 14 samples from the Backlundtoppen Formation and 1 sample from the lower Grusdievbreen Formation.

The filtered Sr isotope data are plotted with the global Neoproterozoic composite of Chen et al. (2022; Figure 12). Although most analyses are slightly more radiogenic than the global record, samples with the lowest $^{87}Sr/^{86}Sr$ within each unit may provide a maximum seawater estimate, as the Sr isotopic composition of carbonates is typically altered to higher values in successions containing siliciclastic sediments (Chen et al., 2022).

C and O isotopes

New $\delta^{13}C$ and $\delta^{18}O$ analyses from carbonates of the Lomfjorden and lower Hinlopenstretet supergroups range from -7.39 – 14.13‰ (one outlier at -12.56) and -12.99 – 3.26 ‰ (multiple outliers), respectively, and agree well with published chemostratigraphic data (Figure DR4; Table DR6; Halverson et al., 2005, 2007a; Cox et al., 2016b). Significant negative carbon isotope excursions are recognized across the Grusdievbreen-Svanbergfjellet contact and within the Russøya Member.

DISCUSSION

Carbonate contamination and effect of filtering on provenance and weathering trends

Ternary diagrams and cross plots of major oxides illustrate the importance of filtering mudrock geochemical data from mixed carbonate-siliciclastic successions when investigating trends in siliciclastic provenance and weathering (Figures 4, 5 & 6). When mudrock samples from the Lomfjorden and lower Hinlopenstretet supergroups with varying carbonate content (variable Ca/Al) are considered, there are moderate to strong positive correlations between Al_2O_3, SiO_2, TiO_2, K_2O and Fe_2O_3, as well as moderate to strong negative correlations between those oxides and CaO and MgO (Figure DR7). However, these trends are driven by samples with high Ca/Al and disappear in a rigorously filtered dataset. Additionally, samples with even small amounts of carbonate (Ca/Al > 0.3 or ~5–10 % carbonate minerals) within this dataset tend to be drawn towards the CaO^*+Na_2O apex on an ACNK diagram (Figure 6), resulting in lower CIA values. This occurs despite the standard correction for Ca in carbonate minerals (e.g., McLennan et al., 1993) and is due in part to the lower Al_2O_3 concentrations in marly mudrocks. On the ACNKFM diagram, typically used to detect the presence of mafic material in sedimentary units, samples with high Ca/Al plot towards that $MgO+FeO_T$ axis, likely a result of the presence of dolomite.

Immobile element ratios that are fractionated during igneous differentiation processes, including HREE/LREE, Eu anomalies, Ti/Al, La/Th, La/Sc, and Th/Sc, are useful in determining the provenance of mudrocks (e.g., McLennan et al., 1993). While these ratios may be robust to weathering processes, it appears that carbonate content can affect them. Mudrock samples in this dataset with high Ca/Al have variable Th/Sc, La/Th, and Eu anomalies (Figures 4 and 10) compared to other mudrock samples from the same stratigraphic unit and tend to be offset in the same direction as carbonate samples from that unit (Figure 7). Mudrocks with high Ca/Al also have lower REE concentrations and ratios that differ from other mudrocks in this dataset (Figure 3). Furthermore, Ca/Al ratios and CaO concentrations correlate negatively with most trace elements that are commonly used in provenance and redox studies (Figure DR11).

While it is possible to discern mudrocks with very high carbonate content in the field, our dataset shows that the geochemistry of mudrocks with even minor carbonate "contamination" (~5–10%) may still be influenced by these phases. Thus, as demonstrated for the Lomfjorden and lower Hinlopenstretet supergroups, rigorous filtering for carbonate-rich samples, ideally with Ca/Al ratios, may be critical to accurately discern provenance and weathering interpretations in mixed carbonate-siliciclastic successions.

Provenance of the Lomfjorden and lower Hinlopenstretet mudrocks

Source characterization

The "provenance and weathering subset" major and trace element data from the Lomfjorden and lower Hinlopenstretet supergroups is remarkably homogenous over more than 6 km of strata and reflects minimal variation in source region (Figures 6 & 7; Figure DR12). Mudrock REE concentrations and ratios, namely high LREE/HREE, and Al/Ti indicate a chemically differentiated source composition (Figures 3 & DR8). Th/Sc (1.0 to 1.2 IQR) and Eu anomalies (0.56 to 0.62 IQR) from these mudrocks are consistent with sediment sourced from a differentiated arc, upper continental crust and/or recycled sedimentary material. While the latter two reservoirs are characterized by Th/Sc ~1 and homogenous Eu anomalies of 0.6–0.7, young differentiated arc material can have more variable Th/Sc and Eu anomalies (0.5–0.9; Figures 7 & 9; McLennan et al., 1993). In contrast, undifferentiated terrains, such as oceanic arcs or LIPs, typically have low Th/Sc and lack significant Eu anomalies ($Eu_n/Eu_n^* \sim 1$). Simple mixing calculations based on trace element ratios constrain the mafic input to be minimal (< 5%) across most of this succession (see Supplemental Material).

While post-depositional K-addition is present in most Precambrian mudrocks (Fedo et al., 1995; Tosca et al., 2010), the most parsimonious interpretation of the major oxide geochemistry of the Lomfjorden and lower Hinlopenstretet supergroups is that the mudrocks were derived from a K-rich granitic source and experienced relatively minimal post-depositional K-addition (see Supplementary Material for further discussion). Mudrock samples plot along a granitic weathering trend on the ACNK diagram and slight deviation from this trend is consistent with minor K-addition (Figure 6). These mudrocks occupy a relatively limited area of the ACNKFM ternary, which is also consistent with a relatively homogenous “granitic” source. Given the lack of correlation between FeO_T+MgO molar proportions and typical trace element ratios characteristic of a mafic source region, individual samples that plot closer to the FeO_T+MgO apex on the ACNKFM ternary are likely the result of syn- or post-depositional Fe addition or un-filtered carbonate contamination. This includes samples from the Oxfordbreen and Grusdievbreen formations, a subset of samples from the Russøya Member collected in the Backlundtoppen area, a subset of samples from the Algal Dolomite member of the Svanbergfjellet Formation (Figure DR13), and samples from the Dracoisen Formation (see Supplementary Material for further discussion).

Whole-rock Sm–Nd isotope chemostratigraphy ($\varepsilon_{Nd(T)}$) of detrital mudstones primarily tracks the age of sediment sources (time since differentiation from a mantle reservoir; McCulloch and Wasserburg, 1978) and responds to changes in the sediment provenance or emplacement of juvenile material in the source region (e.g., Basu et al., 1990; McLennan and Hemming, 1992; McLennan et al., 1993; Turner et al., 1993; Hemming et al., 1995; Condie et al., 2001; Hurowitz and McLennan, 2005). However, both juvenile basalts and granitoids that are the product of mantle melting are characterized by $\varepsilon_{Nd(T)}$ similar to that of depleted upper mantle (Shirey et al., 2008), and their contribution to sediment cannot be resolved with Nd isotopes alone. Combining Nd isotopes with elemental geochemistry is essential to characterizing both the age and geochemical composition of local inputs to a sedimentary basin.

In the Lomfjorden and lower Hinlopenstretet mudrock sample set $\varepsilon_{Nd(T)}$ does not correlate with metrics of igneous differentiation, such as Th/Sc and f_{SmNd}, or concentrations of elements typically higher in mafic rocks (Sc, V, Ni, Co, Cr, Mg; Figures 13 & 14; Tables DR2 & 4), except for in individual samples from the Russøya and Macdonaldryggen members of the Elbobreen Formation discussed below (Figure DR14). This indicates that more juvenile (higher) $\varepsilon_{Nd(T)}$ values are not necessarily driven by increased input of mafic material, as originally proposed by Cox et al. (2016b) based on $\varepsilon_{Nd(T)}$ values alone. Rather, when interpreted along with other geochemical data, $\varepsilon_{Nd(T)}$ values point to a young, chemically differentiated source region. The range of $\varepsilon_{Nd(T)}$, Th/Sc, and f_{SmNd} in this dataset is best explained by multiple sources with a granitic to granodioritic bulk composition, including a relatively juvenile terrane with a higher Nd isotopic signature and an older terrane with a lower signature (Figures 13 & 14). This conclusion is supported by simple mixing calculations based on trace element ratios, $\varepsilon_{Nd(T)}$ values, and Nd concentrations (see Supplementary Material; Figures DR15−17).

Consistent with a chemically differentiated source, mudrocks from the "provenance and weathering subset" mostly plot within the continental arc field on discrimination diagrams (Figure 10). Samples spanning the entire succession have high Zr and Hf concentrations, indicating heavy mineral enrichment; however, the lack of correlation between Zr/Ti (or Zr/Sc) and either $\varepsilon_{Nd(T)}$ (Figure 13) or metrics of chemical maturity, such as CIA_{paleo} (Figure DR10), eliminates recycled sedimentary material as the dominant evolved source of Nd to the Lomfjorden and lower Hinlopenstretet mudrocks. Instead, heavy mineral enrichment could be the product of a zircon-rich source or sedimentary sorting/recycling during transport.

A lower molar proportion of K_2O and higher FeO_T+MgO, along with low Th/Sc, high Ti/Al and elevated MgO (Figures 6, 9 & DR8), point to a greater contribution of mafic material to the mudrocks of the Arena Formation of East Greenland than northeastern Svalbard, as suggested by Kunzmann et al. (2015). While these authors also proposed that the geochemistry of the correlative Macdonaldryggen Member reflects increased mafic sediment contribution, most Macdonaldryggen Member samples with Ca/Al < 0.3 have typical Ti/Al and only slightly lower Th/Sc (~0.9), consistent with the majority of mudrocks from the Lomfjorden and lower Hinlopenstretet supergroups (Table DR2). Furthermore, a clear correlation between elevated Ca/Al and the molar proportion of FeO_T+MgO demonstrates that carbonate contamination affects the geochemistry of the Macdonaldryggen mudrocks. Nevertheless, a small subset of samples from the lower Macdonaldryggen Member (sections G407 and G1647) does have lower Th/Sc (0.4 to

0.6), slightly elevated Ti/Al, relatively high concentrations of trace elements characteristic of a mafic source (e.g., V and Sc), and higher $\varepsilon_{Nd(T)}$ than samples from the middle to upper Macdonaldryggen Member (Figure DR14; Tables DR2 & DR4). Thus, although carbonate contamination is important for the interpretation of Macdonaldryggen mudrocks, it cannot explain all the geochemical variation in this unit. Instead, it is likely that the lower Macdonaldryggen had some mafic source component. Similarly, the geochemistry of the two stratigraphically highest samples from the Russøya Member, SR-239.5 (Ca/Al 0.3−1 subset) and SR-238 are most readily explained by a mafic source. These samples are characterized by a high molar proportion of FeO_T+MgO, Th/Sc < 0.5, Eu anomaly > 0.7, Al/Ti > 0.07, and high $\varepsilon_{Nd(T)}$ values (Figures 6, 7 & 11). Additionally, these samples have high Sc, V, Cr, and Ni concentrations (Figure DR14; Table DR2). A third sample from the Russøya Member has a high $\varepsilon_{Nd(T)}$ signature; however, it has a very high carbonate content (Ca/Al=212) and low concentrations of trace elements.

Potential source regions

Locally, the Lomfjorden Supergroup nonconformably overlies the ca. 960 Ma Kapp Hansteen Group. At its type locality, the Kapp Hansteen Group comprises ~2 km of felsic to intermediate extrusive units intruded by quartz porphyries of the same age (Ohta, 1985). Numerous mafic and felsic igneous rocks from across Nordaustlandet have been correlated with the Kapp Hansteen Group (Ohta, 1985; Gee and Teben'kov, 1996; Johansson et al., 1999). Based on the presence of monomict felsic igneous conglomerates in the basal Galtedalen Group, the Kapp Hansteen Group was exposed at the surface during deposition of the lowermost Lomfjorden Supergroup (Gee and Teben'kov, 1996; Sandelin et al., 2001). Zircon U–Pb ages from the Bogen Member (Zhang et al., 2023) overlap within uncertainty with the magmatic age of the Kapp Hansteen Group and raise the possibility of continued or re-exposure of these units throughout Veteranen Group sedimentation. The majority of samples from the Lomfjorden and lower Hinlopenstretet supergroups have $\varepsilon_{Nd(T)}$ values equal to or lower than the available data for the Kapp Hansteen Group (Figure 11; Johansson et al., 1999, this study), and given that the Kapp Hansteen Group spans the same range of Zr concentrations and Zr/Ti ratios observed in the mudrocks, it can explain the Zr-rich nature of these sediments (Figure 13). The mudrock major and trace element chemistry is mostly consistent with derivation from this local source, although the Kapp Hansteen Group displays a larger range of Th/Sc values, LREE/HREE ratios, and Eu anomalies than the mudrocks (Figures 3, 7 & 9), suggesting a different or additional source with a more granodioritic composition. Additionally, the Kapp Hansteen Group has a narrower range of f_{SmNd} (between -0.2 and -0.4) than the mudrocks (-0.3 to -0.6) and cannot account for either the lowest f_{SmNd} values or evolved $\varepsilon_{Nd(T)}$ values (Figures 11 & 14B), thus requiring an additional source that is more isotopically evolved.

Most paleogeographic reconstructions place the Eastern Svalbard basement domain outboard of Laurentia and adjacent to East Greenland, which has a strikingly similar Neoproterozoic sedimentary succession (Harland, 1997; Sønderholm et al., 2008; Hoffman et al., 2012). The Paleoproterozoic crystalline basement of East Greenland is derived from older, likely Archean, crustal components, which would have evolved to lower isotopic values by the time of deposition of the Lomfjorden and lower Hinlopenstretet supergroups. These rocks have $\varepsilon_{Nd(T)} < -10$ at the time of sedimentation (914–630 Ma) and could explain the more isotopically evolved and lower f_{SmNd} values in some mudrocks (Figures 11, 14B & 15; Kalsbeek et al., 1993). Paleoproterozoic basement is also present in the West Ny Friesland Terrane, west of the ESZ (Figure 1B; Gee et al., 1992; Johansson et al., 1995). Although these units were previously proposed to comprise the basement in East Ny Friesland (Nordaustlandet Terrane), new reconstructions suggest that the ESZ is a major basement boundary and that these units were instead juxtaposed with North Greenland (Bazarnik et al., 2019), making them an unlikely sediment source.

It has also been proposed that the Lomfjorden and Hinlopenstretet supergroups were deposited along the northeastern margin of Laurentia (present coordinates) in the Asgard Sea, a marine basin potentially formed during the rotation of Baltica away from Laurentia in the latest Mesoproterozoic (Cawood et al., 2010). Based primarily on detrital zircon U–Pb geochronology, the Grenville-Sveconorwegian Province, spanning the area from the Great Lakes to southern Scandinavia, was proposed as the main sediment source region to Mesoproterozoic–Neoproterozoic successions deposited in the Asgard Sea, including East Greenland (Kalsbeek et al., 2000; Watt and Thrane, 2001; Kinnaird et al., 2009; Olierook et al., 2020), Scotland (Cawood et al., 2015; Krabbendam et al., 2017), Svalbard (Lorenz et al., 2012; Rainbird et al., 2017; Wala et al., 2021) and Baltoscandia (Bingen et al., 2011).

Southern Laurentia and Baltica (present coordinates) formed a long-lived active margin for much of the Paleoproterozoic–Mesoproterozoic, against which exotic juvenile arc terranes accreted before continental collision with Baltica and Amazonia during the multiphase Elzevirian-Shawinigan-Grenville-Sveconorwegian Orogeny (e.g., Carr et al., 2000; Whitmeyer and Karlstrom, 2007; Bingen et al., 2008, 2021; McLelland et al., 2013; Slagstad et al., 2013). As such, Nd isotope signatures from felsic to intermediate lithologies in the Grenville-Sveconorwegian provinces yield relatively juvenile signatures and are a potential candidate for the source of the chemically differentiated and isotopically juvenile to intermediate Lomfjorden and lower Hinlopenstretet mudrocks (Figures 14 & 15; Table DR8). For example, distinctly juvenile late Mesoproterozoic crust is abundant in the Southwest Grenville Province, comprising the

Adirondacks, Mauricie, Mount Laurier, Rift Zone, and Laurentian areas (Dickin et al., 2010), and accreted arcs of the Quebecia and Quebecia East terranes in the central Grenville Province (Vautour and Dickin, 2019). Grenvillian units with ε_{Nd800} > -5 typically span f_{SmNd} -0.3 to -0.55, very similar to the range in samples from the Lomfjorden and lower Hinlopenstretet supergroups (Figure 14A). Older and more isotopically evolved crust within the Grenville Orogeny has f_{SmNd} between -0.35 and -0.6. While there is limited trace element data from potential Grenvillian sources with Nd isotope data, given their felsic nature (Figure DR18) and the anomalous abundance of detrital zircon from this age in global composites (e.g., Sundell and Macdonald, 2022), juvenile Grenville crust can also explain the Th/Sc ~1 and high Zr observed in the mudrocks.

Granitoids associated with the Sveconorwegian orogeny have $\varepsilon_{Nd(800Ma)}$ between -8 and 0.7, with f_{SmNd} ranging from -0.65 to -0.27 (Figure 14A; Menuge, 1988; Bingen et al., 1993; Welin, 1994; Andersen, 1997; Andersen et al., 2001; Bogaerts et al., 2003; Vander Auwera et al., 2003; Granseth et al., 2020). Such granitoids include the 1070–1010 Ma Sirdal Magmatic Belt, the 1000–920 Ma hornblende-biotite granitoid suite (Slagstad et al., 2018), and the ca. 925 Ma Flá-Idefjord-Bohus suite (Bingen et al., 2008; Granseth et al., 2020). Anorthosites of the ca. 930 Ma Rogaland Igneous Complex (Schärer et al., 1996; Charlier et al., 2007) have slightly more juvenile $\varepsilon_{Nd(800Ma)}$, ranging from -2.7 to 2.5, and have f_{SmNd} between -0.36 and -0.12 (e.g., Bolle et al., 2003). Older and more isotopically evolved material is found in the Meso–Paleoproterozoic Transscandinavian Igneous Belt (e.g., Bingen, 2011). Thus, a combination of units from the Sveconorwegian Orogen can also explain the Nd isotope composition of mudrocks from the Lomfjorden and lower Hinlopenstretet supergroups.

In summary, while the Kapp Hansteen Group and/or juvenile Grenville-Sveconorwegian crust accounts for the intermediate to juvenile $\varepsilon_{Nd(T)}$ values from the Lomfjorden and lower Hinlopenstretet mudrocks, older crust within the Grenville Orogen and East Greenland is needed to explain the more evolved $\varepsilon_{Nd(T)}$ values (Figure 14); thus, a combination of these young and old chemically evolved terranes likely sourced the sediment of these mudrocks.

The most juvenile Nd isotope values in the Lomfjorden and lower Hinlopenstretet supergroups come from the ca. 743 Ma Kinnvika Member (-4.2 to -2.6) and overlying ca. 734 Ma Russøya Member (-2.3 to -1.5), but only the two stratigraphically highest samples in the Russøya Member have geochemical indications of detrital mafic input (e.g., Th/Sc < 0.5; Figures 7 & 11). The Kinnvika Member marks renewed input of siliciclastic material to the carbonate-dominated Akademikerbreen Group and is regarded as a potential subtle stratigraphic marker of renewed extension (Halverson et al., 2018a, 2022; Zhang et al., 2023). This shift in $\varepsilon_{Nd(T)}$ values may provide some geochemical evidence for basin reorganization. Andesitic samples from the Kapp Hansteen Group (25-1 and -2 of Johansson et al., 1999 and J1837 of this study) have lower Th/Sc values and higher concentrations of MgO and mafic trace elements than more felsic units, and have some of the highest $\varepsilon_{Nd(T)}$ values for the Kapp Hansteen Group (Table DR2 and Figure DR19). It is possible that correlated but unsampled local mafic units (i.e., basic dykes of Ohta 1985) would have even higher $\varepsilon_{Nd(T)}$ and lower Th/Sc, explaining the most juvenile and mafic mudrock compositions in the Russøya Member.

The Macdonaldryggen Member and the Dracoisen Formation have the lowest $\varepsilon_{Nd(T)}$ in the Lomfjorden and lower Hinlopenstretet supergroups. The intervening Wilsonbreen Formation diamictite samples have only slightly higher $\varepsilon_{Nd(T)}$ (Cox et al., 2016b), which could be an artefact of the nature of glacial erosion bringing exogenous clasts and material into the drainage. This dataset supports a major provenance shift in northeastern Svalbard around the Tonian-Cryogenian boundary, occurring between the Russøya and Macdonaldryggen members, which represents the largest time-gap in this dataset (Figure 11). The cause of this change is unknown, but it could be related to burial of juvenile units locally or erosion of juvenile terranes in the Grenville Province during the late Tonian or early Cryogenian. A change in the exposed crust could be driven by Cryogenian rifting and erosion of the continental interior, glacial erosion (Keller et al., 2019), or gradual uplift and erosion of older crust through time. The provenance shift in northeastern Svalbard occurs amidst changing global weathering trends, characterized by increasingly radiogenic seawater Sr and Os isotope signatures, that are consistent with an increase in the relative flux of older evolved crustal material (Figure 15; Chen et al., 2022).

Neoproterozoic weathering conditions

Implications for long-term pre-Sturtian basalt weathering hypothesis

Recent geochronological data place the eruption of the Franklin LIP a few million years before the onset of the Sturtian glaciation, bolstering the "Fire and Ice" hypothesis (Pu et al., 2022; Dufour et al., 2023; Macdonald and Swanson-Hysell, 2023). In addition to the proximate cause of glaciation, it has been suggested that long-term weathering of basalts may have driven cooling throughout the Tonian (e.g., Cox et al., 2016b). Although temperature itself is not well constrained in the Neoproterozoic, the sensitivity of radiogenic isotopes to lithologic sources means that they can provide insight into global weathering dynamics.

The Sr isotope composition of carbonate samples from the Lomfjorden and lower Hinlopenstretet supergroups are elevated compared to the global Neoproterozoic curve, likely the result of some diagenetic alteration. Nevertheless, the lowest $^{87}Sr/^{86}Sr$ values obtained from some units are consistent with other global records (Figure 12). These data indicate an increasingly radiogenic seawater $^{87}Sr/^{86}Sr$ composition between ca. 800 and 780 Ma, followed by a decrease leading up to the Sturtian glaciation (Park et al., 2020; Chen et al., 2022), potentially driven by a relative increase in the (unradiogenic) mafic weathering flux. Similarly, the initial Os isotope (Os*i*) record suggests an increasing proportion of mafic weathering globally in the late Tonian, with the Os*i* curve reaching mantle-like values by 732 Ma (Rooney et al., 2014). This contrasts with the more radiogenic Os*i* values from the early–middle Tonian (Figure 15; Van Acken et al., 2013; Rooney et al., 2018; Maloney et al., 2021; Zhang et al., 2023).

The detrital Nd isotope records of Neoproterozoic sedimentary basins provide a complementary dataset that can distinguish between juvenile and evolved crustal material, and if combined with elemental geochemical data, the lithological composition of that source. Based on Nd isotope data from northeastern Svalbard, Cox et al. (2016b) estimated that the fraction of detrital mafic material to the Lomfjorden and lower Hinlopenstretet supergroup mudrocks was significant, implying that flood basalts were the dominant source of REEs. However, as discussed above, our data indicate instead that granitic-granodioritic source(s) were the dominant sediment source in northeastern Svalbard (Figures DR16 & DR17).

Only the two stratigraphically highest samples from the Russøya Member and the samples from the lowest Macdonaldryggen Member have more juvenile $\varepsilon_{Nd(T)}$ and higher concentrations of trace elements potentially sourced from mafic rocks (Figure DR14; Table DR2), which could reflect stratigraphic trends in the late Tonian to Cryogenian detrital source. As discussed above, the geochemistry of the mid-Cryogenian non-glacial Arena Formation of East Greenland reflects mafic input that may have been sourced from the weathering of the Franklin LIP (Kunzmann et al., 2015). In addition to the more proximal Arena Formation, Franklin weathering could explain the elevated $\varepsilon_{Nd(T)}$ and low Th/Sc in the lower Macdonaldryggen Member samples, as most dykes and volcanic units associated with the Franklin LIP have $\varepsilon_{Nd(T)} > 0$ (Dupuy et al., 1995; Shellnutt, 2004; Beard et al., 2017; Dufour, 2022). However, there are no known potential mafic sources to the Russøya Member, whose deposition preceded emplacement of the Franklin LIP by at least 8 million years (Millikin et al., 2022; Zhang et al., 2023). As outlined above, one potential source for these geochemical characteristics in the Russøya Member is yet unsampled mafic units correlated with the Kapp Hansteen Group.

The $\varepsilon_{Nd(T)}$ isotope record of Neoproterozoic strata in Northwest Canada and the southern Canadian Cordillera is similar to that in northeastern Svalbard, with all Tonian mudstone data falling in a relatively radiogenic range between -2.7 and -11, and $\varepsilon_{Nd(T)}$ becoming significantly more radiogenic following the Sturtian glaciation (Figure 15; Table DR9; Boghossian et al., 1996; Rainbird et al., 1997; Cox et al., 2016b). Syn-Sturtian iron formation samples are more juvenile, reaching $\varepsilon_{Nd(T)}$ values ~ 2, however the geochemistry of these samples at least partially reflects hydrogenous REE input from hydrothermal sources (Halverson et al., 2011; Cox et al., 2016a). Based on detrital zircon U–Pb studies, these Neoproterozoic basins received sediment from the dominantly felsic and juvenile crust exposed in the Grenville Province (Rainbird et al., 1997, 2011; Dehler et al., 2017). In fact, low-resolution Nd isotope data yielding relatively juvenile signatures of Mesoproterozoic to early Neoproterozoic strata in Northwest Canada were originally interpreted to reflect this same source (Rainbird et al., 1997). Given our finding that almost all Tonian mudrocks in northeastern Svalbard with relatively juvenile Nd isotope signatures are derived from felsic to intermediate sources, further geochemical data are needed to establish the source of elevated Nd isotope signatures recorded in Laurentian basins across Canada.

Looking beyond Laurentia, elevated $\varepsilon_{Nd(T)}$ data coupled with elevated concentrations of mafic trace elements provide strong evidence for a mafic contribution to Cryogenian mudrocks of central and southern Australia, including the non-glacial Aralka Formation of the Amadeus Basin (Barovich and Foden, 2000; Cox et al., 2016b), and the Appila Tillite and non-glacial Tapley Hill, Etina, and Enamora formations of the Adelaide Geosyncline (Figure 15; Table DR9; Turner et al., 1993; Barovich and Foden, 2000). These units potentially received detritus from the ca. 825 Ma Gairdner/Willouran LIP (Barovich and Foden, 2000), and high $\varepsilon_{Nd(T)}$ values from the Sturtian-aged Chambers Bluff Tillite and Holowilena Iron Formation in the East Officer Basin may also reflect this source (Cox et al., 2016b). However, no accompanying major and trace element data is available for these samples (Wade et al., 2005; Cox et al., 2016b). While there is substantial evidence for mafic detrital input into Cryogenian units across Australia, evidence for relatively juvenile Nd isotope signatures in Tonian strata is more limited. Tonian mudrocks in both the Amadeus and Officer basins have evolved signatures (Zhao et al., 1992; Wade et al., 2005; Cox et al., 2016b), although elevated $\varepsilon_{Nd(T)}$ from the Tonian Burra Group in the Adelaide Geosyncline, coupled with high concentrations of mafic trace elements, point to a potential LIP source (Turner et al., 1993; Barovich and Foden, 2000).

Middle Tonian sedimentary successions from the South China Block record rifting beginning with bimodal volcanism of the ca. 820 Ma Guibei LIP. Elevated sedimentary $\varepsilon_{Nd(T)}$ values, spanning 2.8 to -6.9 (Figure 15; Table DR9), are significantly more juvenile than the basement and represent an increase in the longer-term sedimentary record from South China (Li and McCulloch, 1996). These more juvenile Nd isotope signatures correlate with high concentrations of mafic trace elements and are best explained by regional basalt weathering (Wang et al., 2011).

Taken together, although there is significant evidence for potential LIP weathering in the Cryogenian units discussed above, the Tonian detrital record of LIP weathering is more ambiguous; there is minimal evidence for mafic detritus in late Tonian strata in northeastern Svalbard, consistent with the absence of known Tonian LIPs in Svalbard and eastern Greenland. A major Tonian LIP does occur in the Canadian Cordillera (i.e. the Gunbarrel), but the role of this LIP in sedimentary provenance requires further evaluation with major/trace element geochemistry. Only in South China and the Adelaide Geosyncline is there strong evidence for local LIP and/or mafic detritus in the late Tonian record. Although this work demonstrates that previous suggestions of local LIP weathering in northeastern Svalbard in the middle to late Tonian are equivocal, LIP weathering in other areas may have led to cooling and contributed to the decline in Sr and Os isotope values observed between ca. 780 and 720 Ma that are indicative of increased mafic weathering globally (Figure 15). It has also been proposed that these isotopic signatures reflect weathering of mafic units, such as basalts and ophiolites, in a collisional arc setting rather than a LIP (e.g., Macdonald et al., 2019). Park et al. (2020) argued that the relative amount of weatherable LIP material in the tropics, where global weathering rates are highest, does not increase in the middle to late Tonian and therefore cannot explain the increasingly unradiogenic Sr and Os isotope values across this interval. They proposed instead that declining Sr isotope values were driven by weathering of arc material in the tropics, given a temporal link with oceanic arc accretion in the Arabian-Nubian Shield ca. 780−760 Ma and ca. 730−710 Ma (Johnson et al., 2011).

Weathering intensity in the source region

Mudrock composition and maximum depositional CIA values (corrected for K-addition) were calculated by projecting the measured sample composition onto the granitic weathering trend as outlined in Fedo et al. (1995). The original CIA was maintained when this resulted in a negative correction—i.e., for samples that plot to the K_2O-poor side of the weathering trend (see Supplementary Material for further details). The resulting corrected CIA values (CIA_{paleo}) are a maximum estimate for the given weathering trend and are on average 4.0 units above the original, with a maximum correction of 16.8 units. An alternative possibility is that these mudrocks were derived from a granodioritic source composition and experienced significant K-metasomatism. Although the CIA_{paleo} values are greater if a granodioritic composition is assumed, the relative CIA_{paleo} values within the dataset are relatively constant.

CIA_{paleo} values from the Veteranen Group, Grusdievbreen and Draken formations, and lower Backlundtoppen member, are similar to that of an average shale, spanning 65−85 with the majority between 70−80 (Figure 9; Nesbitt and Young, 1982). MMI is the dominant clay mineral assemblage in these mudrocks, which also contain abundant Fe and Mg chlorite and smectite (Figure 8). Smectite is uncommon in most Precambrian mudrocks, as metamorphism and K-addition typically transform smectite to illite or chlorite (Tosca et al., 2010), so its relative abundance in these mudrocks is consistent with the interpretation that they experienced minimal post-depositional K-addition. Cation-poor weathering products formed during intense leaching, such as kaolinite and iron oxides, are notably absent except in the Svanbergfjellet Formation. Samples from the Svanbergfjellet Formation have the highest CIA_{paleo} values in the succession, consistent with intense chemical leaching during weathering in the source region (Figures 7 & 9). Svanbergfjellet $\varepsilon_{Nd(T)}$ values are more evolved than surrounding units and may reflect the tapping of older crustal sources as the result of extreme weathering conditions. Although there is limited mineralogical data from the Kinnvika and Russøya members, CIA_{paleo} values also indicate a high degree of chemical weathering during deposition of these units.

CIA_{paleo} values for the Macdonaldryggen Member range between 65 and 73 with an average of 71 and those from the Dracoisen Formation range from 54 to 72 with an average of 62 (Figures 7 & 9). These units lie immediately above the Petrovbreen and Wilsonbreen diamictites, respectively, and record low latitude deglaciation, which requires elevated CO_2 to overcome the strong ice-albedo feedback (Pierrehumbert, 2004). Intense chemical leaching and an extreme greenhouse climate would be expected under a CO_2-rich atmosphere with acidic rain, river, and groundwater, especially with abundant physically weathered rock flour that should be susceptible to chemical weathering (Higgins and Schrag, 2003; Fabre and Berger, 2012). The global Os*i* record, including data from the Dracoisen Formation, supports a strong continental weathering flux during both Sturtian and Marinoan deglaciation, reaching radiogenic values that are unmatched in the Precambrian open-ocean record (Figure 15F; Rooney et al., 2015, 2020; Millikin et al., 2022). CIA_{paleo} range in the Macdonaldryggen Member is typical of average shale values and consistent with other post-Sturtian units from South China and Australia (Rose et al., 2013; Wang et al., 2020). In contrast, CIA_{paleo} values from the Dracoisen Formation are lower than in contemporaneous post-Marinoan units (e.g., Rose et al., 2013) and are typical of environments dominated by physical weathering, suggesting that erosion may have outpaced soil formation (and sediment residence time in fluvial systems was low). The elemental chemistry of these mudrocks therefore either reflects local weathering conditions that are likely not representative of contemporaneous weathering conditions globally, or global weathering was dynamic in the wake of snowball glaciation and high chemical weathering rates were not sustained.

Implications of mudrock composition for exceptional microfossil preservation within the Svanbergfjellet Formation

Fossiliferous strata are described throughout the Lomfjorden and lower Hinlopenstretet supergroups (e.g., Knoll, 1982; Knoll and Calder, 1983; Knoll and Swett, 1985; Swett and Knoll, 1985; Knoll et al., 1986, 1991; Riedman et al., 2018). The ca. 790 Ma Algal Dolomite member of the Svanbergfjellet Formation in particular has yielded remarkable organic-walled micro- and macro-fossils (Butterfield et al., 1994; Mughal et al., 2025) and is considered a Neoproterozoic Lagerstätte (Butterfield, 1995), with fossils like *Proterocladus* and *Palaeastrum* informing the Tonian diversification of eukaryotes (Butterfield et al., 1988, 1994; Mughal et al., 2025). Interestingly, the Algal Dolomite member is also geochemically unique among strata in the Lomfjorden and lower Hinlopenstretet supergroups with extremely low Ti/Al ratios and low Zr concentrations (Figures 10 & DR8), as well as high concentrations of Al_2O_3, K_2O, and REEs (Figure 6; Table DR2). These geochemical data indicate enrichment in clays and depletion in heavy minerals, potentially during intense chemical weathering or physical sorting. Although the Algal Dolomite member was deposited in a similar environment to bounding strata (Halverson et al., 2018a), it is the only interval in the Lomfjorden or lower Hinlopenstretet supergroups with these geochemical characteristics, suggesting that it records a unique climatic signal. This inference is corroborated by the high CIA_{paleo} values in this unit and the abundance of kaolinite (Figures 7, 8 & 9).

The Algal Dolomite member is composed of cyclical packages of meter- to decameter-scale stromatolitic biostromes/bioherms and exceptionally preserved fossils derive from subtidal calcareous shale and siltstone that sit directly on top of these biostromes/bioherms (Butterfield et al., 1994; Mughal et al., 2025). The member likely records predominantly subtidal environments with some protection from storm or wave action (Knoll and Swett, 1990). Sharp contacts between stromatolitic buildups and fossiliferous mudrocks record potential rapid flooding and/or avulsion events leading to siliciclastic-dominated sedimentation. High resolution sections measured through fossiliferous mudrocks at De Geerbukta (Mughal et al., 2025) reveal that the molar proportion of FeO_T+MgO, Fe/Al and the relative proportion of cation-rich clays to kaolinite increases from the bottom to the middle or top of the mudrock intervals (Figure DR13). Given that Fe/Al is poorly correlated with both Ca/Al and Ti/Al, it is unlikely that these shale-to-stromatolite cycles reflect varying siliciclastic input (Table DR2). Instead, the trend of increasing Fe/Al up-section could reflect deepening to a maximum flooding surface across a redoxcline. This is consistent with the redox structure of other middle Tonian basins, such as that recorded in the Fifteenmile Group of Northwest Canada, characterized by Fe enrichment in anoxic deepwater overlain by oxygenated shallow environments (Sperling et al., 2013; Gibson et al., 2020). Despite these trends, there is no correlation between fossil abundance or diversity (Mughal et al., 2025) and geochemical or mineralogical parameters in these high resolution sections.

The Algal Dolomite member is unique among the strata of the Lomfjorden and lower Hinlopenstretet supergroups in being the only unit to record significant kaolinite, which is likely linked to the exceptional preservation of fossils in this unit (Figure 8). Kaolinite has been documented in direct association with Burgess Shale-type fossils (Orr et al., 1998; R. Anderson et al., 2021). Anderson et al. (2020) reported that fossils from the Algal Dolomite member are surrounded by aluminum-rich haloes, which likely represent kaolinite. Kaolinite is known to aid preservation due to its toxicity to microbial degraders (McMahon et al., 2016) and by promoting the transformation of organic remains to more decay-resistant compounds (Wilson and Butterfield, 2014). Fe-rich clays are abundant throughout the Lomfjorden and lower Hinlopenstretet supergroups, and likely also played a role in the Algal Dolomite member's exceptional fossil preservation. Fe-bearing clays have been recovered from Cambrian Burgess Shale-type deposits globally (Anderson et al., 2018), where the clay may play a mechanistic role in preservation by (i) decreasing permeability (Woltz et al., 2023), (ii) promoting toxicity to heterotrophic bacteria (McMahon et al., 2016), and/or (iii) forming chemical bonds with the decaying organics (Petrovich, 2001). Regardless of the exact mechanism, the occurrence of exceptional fossil preservation in the Algal Dolomite member suggests a link to the unique intense chemical weathering recorded in this unit.

CONCLUSIONS

Carbonate contamination clearly affects the geochemistry of Lomfjorden and lower Hinlopenstretet mudrocks, highlighting the importance of using major and trace element data and mineralogy to filter datasets and inform provenance interpretations in mixed carbonate-siliciclastic successions. When adequately filtered, the geochemistry and mineralogy of these mudrocks reflect derivation from a combination of young and old differentiated crustal sources, possibly in the Grenville-Sveconorwegian Orogen, East Greenland, or locally via the underlying Tonian Kapp Hansteen Group. By combining Nd isotope analysis with elemental geochemistry, we find little evidence for a mafic detrital source component in Neoproterozoic strata from northeastern Svalbard, except in a couple of rare instances in the Russøya and Macdonaldryggen members of the Elbobreen Formation. This conclusion differs from a previous study that used Nd isotopes alone to support a model of elevated rates of LIP weathering in the Tonian of northeastern Svalbard, highlighting that juvenile isotopic signatures may yield a non-unique provenance and underscoring the importance of evaluating isotopic measurements within the context of elemental and mineralogical data. While the detrital mudrock record from northeastern Svalbard does not record evidence of basaltic weathering throughout the early–middle Neoproterozoic, existing Nd isotope records provide evidence for weathering of the ca. 825 Ma Willouran and Guibei LIPs; however, such a record from the ca. 780 Gunbarrel LIP remains unresolved. Additional work is needed to resolve the climatic conditions and relative influence of basaltic and arc weathering leading into the Sturtian Snowball Earth event. In addition to provenance interpretations from this important Neoproterozoic succession, the integrated geochemical and mineralogical datasets presented herein provide rare insight into the uniqueness of the Algal Dolomite member within the Lomfjorden and lower Hinlopenstretet supergroups and suggest a link between intense chemical weathering conditions and exceptional fossil preservation in this unit.

[1]Supplementary Material. Detailed information about analytical methodology, the composite stratigraphic section and age model used, data filtering, and mixing model calculations. Data tables containing all geochemical and mineralogical data generated and compiled in this study. Please visit https://doi.org/10.1130/XXXX to access the supplemental material, and contact editing@geosociety.org with any questions.

ACKNOWLEDGMENTS

Field work was supported by a National Geographic Society grant (CP-129R-17) awarded to J.V.S., a Royal Society Research Grant (RSG/R1/180077) awarded to R.P.A., and grants from the Yale Institute for Biospheric Studies, Geological Society of America, and Lewis and Clark Fund for Exploration and Field Research awarded to A.E.G.M. This work was supported by U.S. National Science Foundation grants awarded to J.V.S. (EAR-1929593) and A.D.R. (EAR-

1929597). T.M.G. was supported by a Postdoctoral Fellowship from the Agouron Institute and by NSF grant EAR-1929597. N.J.T. was supported by the UK Natural Environment Research Council (NE/M00578X/1) and the Leverhulme Trust (PLP-2015-286). R.P.A. was supported by All Souls College and the Royal Society (URF\R1\221220, RF\ERE\221057). Research was permitted under the Research in Svalbard (RIS) ID #11035. We thank Trond Aasvoll for safe passage around Svalbard in the S/Y Arctica. We thank T. Mackey, J. Creveling, J. Wilcots, M. Cantine, A. Jost, and J. Cooper for assistance in the field, K. Clayton, C. Hayhow, S. Anseeuw, S. Shipman and co-authors on the linked Zenodo repository for laboratory assistance, and S. Shipman, A. Bauer, B. Beatty, S. Mughal, F. Meyer, and K. Piepjohn for helpful discussions. This manuscript was significantly improved by comments from Ian Fairchild and Ross Stevenson.

REFERENCES

Andersen, T., 1997, Radiogenic isotope systematics of the Herefoss granite, South Norway: an indicator of Sveconorwegian (Grenvillian) crustal evolution in the Baltic Shield: Chemical Geology, v. 135, p. 139–158, doi:10.1016/S0009-2541(96)00095-2.

Andersen, T., Andresen, A., and Sylvester, A.G., 2001, Nature and distribution of deep crustal reservoirs in the southwestern part of the Baltic Shield: Evidence from Nd, Sr and Pb isotope data on late Sveconorwegian granites: Journal of the Geological Society, v. 158, p. 253–267, doi:10.1144/jgs.158.2.253.

Anderson, N.T. et al., 2021a, A Unified Clumped Isotope Thermometer Calibration (0.5–1,100°C) Using Carbonate-Based Standardization: Geophysical Research Letters, v. 48, p. e2020GL092069, doi:10.1029/2020GL092069.

Anderson, R.P., Tosca, N.J., Cinque, G., Frogley, M.D., Lekkas, I., Akey, A., Hughes, G.M., Bergmann, K.D., Knoll, A.H., and Briggs, D.E.G., 2020, Aluminosilicate haloes preserve complex life approximately 800 million years ago: Interface Focus, v. 10, p. 20200011, doi:10.1098/rsfs.2020.0011.

Anderson, R.P., Tosca, N.J., Gaines, R.R., Mongiardino Koch, N., and Briggs, D.E.G., 2018, A mineralogical signature for Burgess Shale–type fossilization: Geology, v. 46, p. 347–350, doi:10.1130/G39941.1.

Anderson, R.P., Tosca, N.J., Saupe, E.E., Wade, J., and Briggs, D.E.G., 2021b, Early formation and taphonomic significance of kaolinite associated with Burgess Shale fossils: Geology, v. 49, p. 355–359, doi:10.1130/G48067.1.

Bailey, T.R., McArthur, J.M., Prince, H., and Thirlwall, M.F., 2000, Dissolution methods for strontium isotope stratigraphy: whole rock analysis: Chemical Geology, v. 167, p. 313–319, doi:10.1016/S0009-2541(99)00235-1.

Bao, H., Fairchild, I.J., Wynn, P.M., and Spötl, C., 2009, Stretching the Envelope of Past Surface Environments: Neoproterozoic Glacial Lakes from Svalbard: Science, v. 323, p. 119–122, doi:10.1126/science.1165373.

Barovich, K., and Foden, J., 2000, A Neoproterozoic flood basalt province in southern-central Australia: geochemical and Nd isotope evidence from basin fill: Precambrian Research, v. 100, p. 213–234, doi:10.1016/S0301-9268(99)00075-3.

Basu, A.R., Sharma, M., and DeCelles, P.G., 1990, Nd, Sr-isotopic provenance and trace element geochemistry of Amazonian foreland basin fluvial sands, Bolivia and Peru: implications for ensialic Andean orogeny: Earth and Planetary Science Letters, v. 100, p. 1–17, doi:10.1016/0012-821X(90)90172-T.

Bazarnik, J., Majka, J., McClelland, W.C., Strauss, J.V., Kośmińska, K., Piepjohn, K., Elvevold, S., Czupyt, Z., and Mikuš, T., 2019, U-Pb zircon dating of metaigneous rocks from the

Nordbreen Nappe of Svalbard's Ny-Friesland suggests their affinity to Northeast Greenland: Terra Nova, v. 31, p. 518–526, doi:10.1111/ter.12422.

Beard, C.D., Scoates, J.S., Weis, D., Bédard, J.H., and Dell'Oro, T.A., 2017, Geochemistry and Origin of the Neoproterozoic Natkusiak Flood Basalts and Related Franklin Sills, Victoria Island, Arctic Canada: Journal of Petrology, v. 58, p. 2191–2220, doi:10.1093/petrology/egy004.

Bellefroid, E.J., Planavsky, N.J., Miller, N.R., Brand, U., and Wang, C., 2018, Case studies on the utility of sequential carbonate leaching for radiogenic strontium isotope analysis: Chemical Geology, v. 497, p. 88–99, doi:10.1016/j.chemgeo.2018.08.025.

Bergmann, K. et al., 2024, Svalbard Neoproterozoic–Ordovician $\delta^{13}C$ and $\delta^{18}O$ Isotope Data:, doi:10.5281/zenodo.14276720.

Bhatia, M.R., and Crook, K.A.W., 1986, Trace element characteristics of graywackes and tectonic setting discrimination of sedimentary basins: Contributions to Mineralogy and Petrology, v. 92, p. 181–193, doi:10.1007/BF00375292.

Bingen, B., Belousova, E.A., and Griffin, W.L., 2011, Neoproterozoic recycling of the Sveconorwegian orogenic belt: Detrital-zircon data from the Sparagmite basins in the Scandinavian Caledonides: Precambrian Research, v. 189, p. 347–367, doi:10.1016/j.precamres.2011.07.005.

Bingen, B., Demaiffe, D., Hertogen, J., Weis, D., and Michot, J., 1993, K-Rich Calc-Alkaline Augen Gneisses of Grenvillian Age in SW Norway: Mingling of Mantle-Derived and Crustal Components: The Journal of Geology, v. 101, p. 763–778, doi:10.1086/648273.

Bingen, B., Nordgulen, Ø., and Viola, G., 2008, A four-phase model for the Sveconorwegian orogeny, SW Scandinavia: Norwegian Journal of Geology, v. 88, p. 43–72.

Bingen, B., Viola, G., Möller, C., Vander Auwera, J., Laurent, A., and Keewook, Y., 2021, The Sveconorwegian orogeny: Gondwana Research, v. 90, p. 273–313, doi:10.1016/j.gr.2020.10.014.

Bogaerts, M., Scaillet, B., Liégeois, J.-P., and Vander Auwera, J., 2003, Petrology and geochemistry of the Lyngdal granodiorite (Southern Norway) and the role of fractional crystallisation in the genesis of Proterozoic ferro-potassic A-type granites: Precambrian Research, v. 124, p. 149–184, doi:10.1016/S0301-9268(03)00085-8.

Boghossian, N.D., Patchett, P.J., Ross, G.M., and Gehrels, G.E., 1996, Nd Isotopes and the Source of Sediments in the Miogeocline of the Canadian Cordillera: The Journal of Geology, v. 104, p. 259–277.

Bolle, O., Demaiffe, D., and Duchesne, J.-C., 2003, Petrogenesis of jotunitic and acidic members of an AMC suite (Rogaland anorthosite province, SW Norway): a Sr and Nd isotopic assessment: Precambrian Research, v. 124, p. 185–214, doi:10.1016/S0301-9268(03)00086-X.

Butterfield, N.J., 1995, Secular distribution of Burgess-Shale-type preservation: Lethaia, v. 28, p. 1–13, doi:10.1111/j.1502-3931.1995.tb01587.x.

Butterfield, N.J., Knoll, A.H., and Swett, K., 1988, Exceptional preservation of fossils in an Upper Proterozoic shale: Nature, v. 334, p. 424–427, doi:10.1038/334424a0.

Butterfield, N.J., Knoll, A.H., and Swett, K., 1994, Paleobiology of the Neoproterozoic Svanbergfjellet Formation, Spitsbergen: Fossils and Strata, v. 34, p. 1–84, doi:10.18261/8200376494-1994-01.

Carr, S.D., Easton, R.M., Jamieson, R.A., and Culshaw, N.G., 2000, Geologic transect across the Grenville orogen of Ontario and New York: Canadian Journal of Earth Sciences, v. 37, p. 193–216, doi:10.1139/e99-074.

Cawood, P.A., Strachan, R., Cutts, K., Kinny, P.D., Hand, M., and Pisarevsky, S., 2010, Neoproterozoic orogeny along the margin of Rodinia: Valhalla orogen, North Atlantic: Geology, v. 38, p. 99–102, doi:10.1130/G30450.1.

Cawood, P.A., Strachan, R.A., Merle, R.E., Millar, I.L., Loewy, S.L., Dalziel, I.W.D., Kinny, P.D., Jourdan, F., Nemchin, A.A., and Connelly, J.N., 2015, Neoproterozoic to early Paleozoic extensional and compressional history of East Laurentian margin sequences: The Moine Supergroup, Scottish Caledonides: Geological Society of America Bulletin, v. 127, p. 349–371, doi:10.1130/B31068.1.

Chakrabarti, R., Knoll, A.H., Jacobsen, S.B., and Fischer, W.W., 2012, Si isotope variability in Proterozoic cherts: Geochimica et Cosmochimica Acta, v. 91, p. 187–201, doi:10.1016/j.gca.2012.05.025.

Charlier, B., Ska, Ø., Duchesne, J.-C., and Vander Auwera, J., 2007, Ilmenite composition in the Tellnes Fe–Ti deposit, SW Norway: fractional crystallization, postcumulus evolution and ilmenite–zircon relation: Contributions to Mineralogy and Petrology, v. 154, p. 119–134.

Chen, X., Zhou, Y., and Shields, G.A., 2022, Progress towards an improved Precambrian seawater $^{87}Sr/^{86}Sr$ curve: Earth-Science Reviews, v. 224, p. 103869, doi:10.1016/j.earscirev.2021.103869.

Cohen, P.A., and Macdonald, F.A., 2015, The Proterozoic Record of Eukaryotes: Paleobiology, v. 41, p. 610–632, doi:10.1017/pab.2015.25.

Cole, D.B., Reinhard, C.T., Wang, X., Gueguen, B., Halverson, G.P., Gibson, T., Hodgskiss, M.S.W., McKenzie, N.R., Lyons, T.W., and Planavsky, N.J., 2016, A shale-hosted Cr isotope record of low atmospheric oxygen during the Proterozoic: Geology, v. 44, p. 555–558, doi:10.1130/G37787.1.

Condie, K.C., Lee, D., and Farmer, G.L., 2001, Tectonic setting and provenance of the Neoproterozoic Uinta Mountain and Big Cottonwood groups, northern Utah: constraints from geochemistry, Nd isotopes, and detrital modes: Sedimentary Geology, v. 141–142, p. 443–464, doi:10.1016/S0037-0738(01)00086-0.

Cox, G.M., Halverson, G.P., Poirier, A., Le Heron, D., Strauss, J.V., and Stevenson, R., 2016a, A model for Cryogenian iron formation: Earth and Planetary Science Letters, v. 433, p. 280–292, doi:10.1016/j.epsl.2015.11.003.

Cox, G.M., Halverson, G.P., Stevenson, R.K., Vokaty, M., Poirier, A., Kunzmann, M., Li, Z.-X., Denyszyn, S.W., Strauss, J.V., and Macdonald, F.A., 2016b, Continental flood basalt weathering as a trigger for Neoproterozoic Snowball Earth: Earth and Planetary Science Letters, v. 446, p. 89–99, doi:10.1016/j.epsl.2016.04.016.

Daëron, M., 2023, D47crunch:, https://doi.org/10.5281/zenodo.8407876.

Dallmann, W.K., 2015, Geoscience atlas of Svalbard: Norsk Polarinstitutt, Report Series No. 148, 281 p.

Dehler, C., Gehrels, G., Porter, S., Heizler, M., Karlstrom, K., Cox, G., Crossey, L., and Timmons, M., 2017, Synthesis of the 780–740 Ma Chuar, Uinta Mountain, and Pahrump (ChUMP) groups, western USA: Implications for Laurentia-wide cratonic marine basins: Geological Society of America Bulletin, v. 129, doi:10.1130/B31532.1.

Dessert, C., Dupré, B., François, L.M., Schott, J., Gaillardet, J., Chakrapani, G., and Bajpai, S., 2001, Erosion of Deccan Traps determined by river geochemistry: impact on the global climate and the 87Sr/86Sr ratio of seawater: Earth and Planetary Science Letters, v. 188, p. 459–474, doi:10.1016/S0012-821X(01)00317-X.

Dickin, A.P., McNutt, R.H., Martin, C., and Guo, A., 2010, The extent of juvenile crust in the Grenville Province: Nd isotope evidence: Geological Society of America Bulletin, v. 122, p. 870–883, doi:10.1130/B26381.1.

Donnadieu, Y., Goddéris, Y., Ramstein, G., Nédélec, A., and Meert, J., 2004, A ‘snowball Earth’ climate triggered by continental break-up through changes in runoff: Nature, v. 428, p. 303–306, doi:10.1038/nature02408.

Dufour, F., 2022, Géochronologie et géochimie des roches mafiques du nord du Canada, du bassin de Fury et Hecla au Nunavut, et du bassin de Thulé au Groenland : implications pour les larges provinces ignées de Mackenzie et Franklin [Master’s Thesis]: Université du Québec à Montréal, 197 p.

Dufour, F., Davies, J.H.F.L., Greenman, J.W., Skulski, T., Halverson, G.P., and Stevenson, R., 2023, New U-Pb CA-ID TIMS zircon ages implicate the Franklin LIP as the proximal trigger for the Sturtian Snowball Earth event: Earth and Planetary Science Letters, v. 618, p. 118259, doi:10.1016/j.epsl.2023.118259.

Dupuy, C., Michard, A., Dostal, J., Dautel, D., and Baragar, W.R.A., 1995, Isotope and trace-element geochemistry of Proterozoic Natkusiak flood basalts from the northwestern Canadian Shield: Chemical Geology, v. 120, p. 15–25, doi:10.1016/0009-2541(94)00128-U.

Ernst, R.E., Wingate, M.T.D., Buchan, K.L., and Li, Z.X., 2008, Global record of 1600–700Ma Large Igneous Provinces (LIPs): Implications for the reconstruction of the proposed Nuna (Columbia) and Rodinia supercontinents: Precambrian Research, v. 160, p. 159–178, doi:10.1016/j.precamres.2007.04.019.

Ernst, R.E., and Youbi, N., 2017, How Large Igneous Provinces affect global climate, sometimes cause mass extinctions, and represent natural markers in the geological record: Palaeogeography, Palaeoclimatology, Palaeoecology, v. 478, p. 30–52, doi:10.1016/j.palaeo.2017.03.014.

Fabre, S., and Berger, G., 2012, How tillite weathering during the snowball Earth aftermath induced cap carbonate deposition: Geology, v. 40, p. 1027–1030, doi:10.1130/G33340.1.

Fairchild, I.J. et al., 2016, The Late Cryogenian Warm Interval, NE Svalbard: Chemostratigraphy and genesis: Precambrian Research, v. 281, p. 128–154, doi:10.1016/j.precamres.2016.05.013.

Fairchild, I.J., Hambrey, M.J., Spiro, B., and Jefferson, T.H., 1989, Late Proterozoic glacial carbonates in northeast Spitsbergen: new insights into the carbonate–tillite association: Geological Magazine, v. 126, p. 469–490, doi:10.1017/S0016756800022809.

Fairchild, I.J., and Spiro, B., 1990, Carbonate minerals in glacial sediments: geochemical clues to palaeoenvironment: Geological Society, London, Special Publications, v. 53, p. 201–216, doi:10.1144/GSL.SP.1990.053.01.11.

Fedo, C.M., Nesbitt, H.W., and Young, G.M., 1995, Unraveling the effects of potassium metasomatism in sedimentary rocks and paleosols, with implications for paleoweathering conditions and provenance: Geology, v. 23, p. 921–924, doi:10.1130/0091-7613(1995)023<0921:UTEOPM>2.3.CO;2.

Floyd, P.A., and Leveridge, B.E., 1987, Tectonic Environment of the Devonian Gramscatho Basin South Cornwall: Framework Mode and Geochemical Evidence from Turbiditic Sandstones: Journal of the Geological Society (London), v. 144, p. 531–542, doi:10.1144/gsjgs.144.4.0531.

Gee, D.G., Johansson, Å., Ohta, Y., Tebenkov, A.M., Krasil’s̨c̨hikov, A.A., Balashov, Y.A., Larionov, A.N., Gannibal, L.F., and Ryungenen, G.I., 1995, Grenvillian basement and a major unconformity within the Caledonides of Nordaustlandet, Svalbard: Precambrian Research, v. 70, p. 215–234, doi:10.1016/0301-9268(94)00041-O.

Gee, D.G., Schouenborg, B., Peucat, J.-J., Abakumov, S.A., Krasil’ščikov, A.A., and Tebenkov, A., 1992, New evidence of basement In the Svalbard Caledonides: Early Proterozoic zircon ages from Ny Friesland granites: Norsk Geologisk Tidsskrift, v. 72, p. 181–190.

Gee, D.G., and Teben’kov, A.M., 1996, Two major unconformities beneath the Neoproterozoic Murchisonfjorden Supergroup in the Caledonides of central Nordaustlandet , Svalbard: Polar Research, v. 15, p. 81–91, doi:10.1111/j.1751-8369.1996.tb00460.x.

Gibson, T.M., Kunzmann, M., Poirier, A., Schumann, D., Tosca, N.J., and Halverson, G.P., 2020, Geochemical signatures of transgressive shale intervals from the 811 Ma Fifteenmile Group in Yukon, Canada: Disentangling sedimentary redox cycling from weathering alteration: Geochimica et Cosmochimica Acta, v. 280, p. 161–184, doi:10.1016/j.gca.2020.04.013.

Gibson, T.M., Millikin, A.E.G., Anderson, R.P., Myrow, P.M., Rooney, A.D., and Strauss, J.V., 2021, Tonian deltaic and storm-influenced marine sedimentation on the edge of Laurentia: The Veteranen Group of northeastern Spitsbergen, Svalbard: Sedimentary Geology, v. 426, p. 106011, doi:10.1016/j.sedgeo.2021.106011.

Goddéris, Y., Donnadieu, Y., Nédélec, A., Dupré, B., Dessert, C., Grard, A., Ramstein, G., and François, L.M., 2003, The Sturtian ‘snowball’ glaciation: fire and ice: Earth and Planetary Science Letters, v. 211, p. 1–12, doi:10.1016/S0012-821X(03)00197-3.

Goldstein, S.L., O’Nions, R.K., and Hamilton, P.J., 1984, A Sm-Nd isotopic study of atmospheric dusts and particulates from major river systems: Earth and Planetary Science Letters, v. 70, p. 221–236, doi:10.1016/0012-821X(84)90007-4.

Granseth, A., Slagstad, T., Coint, N., Roberts, N.M.W., Røhr, T.S., and Sørensen, B.E., 2020, Tectonomagmatic evolution of the Sveconorwegian orogen recorded in the chemical and isotopic compositions of 1070–920 Ma granitoids: Precambrian Research, v. 340, p. 105527, doi:10.1016/j.precamres.2019.105527.

Halverson, G.P., Dudás, F.Ö., Maloof, A.C., and Bowring, S.A., 2007a, Evolution of the $^{87}Sr/^{86}Sr$ composition of Neoproterozoic seawater: Palaeogeography, Palaeoclimatology, Palaeoecology, v. 256, p. 103–129, doi:10.1016/j.palaeo.2007.02.028.

Halverson, G.P., Hoffman, P.F., Schrag, D.P., Maloof, A.C., and Rice, A.H.N., 2005, Toward a Neoproterozoic composite carbon-isotope record: Geological Society of America Bulletin, v. 117, p. 1181, doi:10.1130/B25630.1.

Halverson, G.P., Kunzmann, M., Strauss, J.V., and Maloof, A.C., 2018a, The Tonian-Cryogenian transition in Northeastern Svalbard: Precambrian Research, v. 319, p. 79–95, doi:10.1016/j.precamres.2017.12.010.

Halverson, G.P., Maloof, A.C., and Hoffman, P.F., 2004, The Marinoan glaciation (Neoproterozoic) in northeast Svalbard: Basin Research, v. 16, p. 297–324, doi:10.1111/j.1365-2117.2004.00234.x.

Halverson, G.P., Maloof, A.C., Schrag, D.P., Dudás, F.Ö., and Hurtgen, M., 2007b, Stratigraphy and geochemistry of a ca 800 Ma negative carbon isotope interval in northeastern Svalbard: Chemical Geology, v. 237, p. 5–27, doi:10.1016/j.chemgeo.2006.06.013.

Halverson, G.P., Poitrasson, F., Hoffman, P.F., Nédélec, A., Montel, J.-M., and Kirby, J., 2011, Fe isotope and trace element geochemistry of the Neoproterozoic syn-glacial Rapitan iron formation: Earth and Planetary Science Letters, v. 309, p. 100–112, doi:10.1016/j.epsl.2011.06.021.

Halverson, G.P., Porter, S.M., and Gibson, T.M., 2018b, Dating the late Proterozoic stratigraphic record (T. W. Lyons, M. L. Droser, K. V. Lau, & S. M. Porter, Eds.): Emerging Topics in Life Sciences, v. 2, p. 137–147, doi:10.1042/ETLS20170167.

Halverson, G.P., Shen, C., Davies, J.H.F.L., and Wu, L., 2022, A Bayesian Approach to Inferring Depositional Ages Applied to a Late Tonian Reference Section in Svalbard: Frontiers in Earth Science, v. 10, p. 798739, doi:10.3389/feart.2022.798739.

Harland, W.B., 1997, Proto-basement in Svalbard: Polar Research, v. 16, p. 123–147, doi:10.3402/polar.v16i2.6631.

Harland, W.B., Wallis, R.H., and Gayer, R.A., 1966, A Revision of the Lower Hecla Hoek Succession in Central North Spitsbergen and Correlation Elsewhere: Geological Magazine, v. 103, p. 70–97, doi:10.1017/S0016756800050433.

Harland, W.B., and Wilson, C.B., 1956, The Hecla Hoek Succession in Ny Friesland, Spitsbergen: Geological Magazine, v. 93, p. 265–286, doi:10.1017/S0016756800066693.

Hemming, S., McLennan, S., and Hanson, G., 1995, Geochemical and Nd/Pb isotopic evidence for the provenance of the Early Proterozoic Virginia Formation, Minnesota. Implications for the tectonic setting of the Animikie Basin: The Journal of Geology, v. 103, p. 147–168.

Higgins, J.A., and Schrag, D.P., 2003, Aftermath of a snowball Earth: Geochemistry, Geophysics, Geosystems, v. 4, p. 2002GC000403, doi:10.1029/2002GC000403.

Hoffman, P.F., Halverson, G.P., Domack, E.W., Maloof, A.C., Swanson-Hysell, N.L., and Cox, G.M., 2012, Cryogenian glaciations on the southern tropical paleomargin of Laurentia (NE Svalbard and East Greenland), and a primary origin for the upper Russøya (Islay) carbon isotope excursion: Precambrian Research, v. 206–207, p. 137–158, doi:10.1016/j.precamres.2012.02.018.

Hurowitz, J.A., and McLennan, S.M., 2005, Geochemistry of Cambro-Ordovician Sedimentary Rocks of the Northeastern United States: Changes in Sediment Sources at the Onset of Taconian Orogenesis: The Journal of Geology, v. 113, p. 571–587, doi:10.1086/431910.

Ibarra, D.E., Caves, J.K., Moon, S., Thomas, D.L., Hartmann, J., Chamberlain, C.P., and Maher, K., 2016, Differential weathering of basaltic and granitic catchments from concentration–discharge relationships: Geochimica et Cosmochimica Acta, v. 190, p. 265–293, doi:10.1016/j.gca.2016.07.006.

Johansson, Å., Gee, D.G., Björklund, L., and Witt-Nilsson, P., 1995, Isotope studies of granitoids from the Bangenhuk Formation, Ny Friesland Caledonides, Svalbard: Geological Magazine, v. 132, p. 303–320, doi:10.1017/S0016756800013625.

Johansson, Å., Gee, D.G., Larionov, A.N., Ohta, Y., and Tebenkov, A.M., 2005, Grenvillian and Caledonian evolution of eastern Svalbard – a tale of two orogenies: Terra Nova, v. 17, p. 317–325, doi:10.1111/j.1365-3121.2005.00616.x.

Johansson, Å., Larionov, A.N., Tebenkov, A.M., Gee, D.G., Whitehouse, M.J., and Vestin, J., 1999, Grenvillian magmatism of western and central Nordaustlandet, northeastern Svalbard: Transactions of the Royal Society of Edinburgh: Earth Sciences, v. 90, p. 221–254, doi:10.1017/S0263593300002583.

Johnson, P.R., Andresen, A., Collins, A.S., Fowler, A.R., Fritz, H., Ghebreab, W., Kusky, T., and Stern, R.J., 2011, Late Cryogenian–Ediacaran history of the Arabian–Nubian Shield: A review of depositional, plutonic, structural, and tectonic events in the closing stages of the northern East African Orogen: Journal of African Earth Sciences, v. 61, p. 167–232, doi:10.1016/j.jafrearsci.2011.07.003.

Kalsbeek, F., Nutman, A.P., and Taylor, P.N., 1993, Palaeoproterozoic basement province in the Caledonian fold belt of North-East Greenland: Precambrian Research, v. 63, p. 163–178, doi:10.1016/0301-9268(93)90010-Y.

Kalsbeek, F., Thrane, K., Nutman, A.P., and Jepsen, H.F., 2000, Late Mesoproterozoic to early Neoproterozoic history of the East Greenland Caledonides: evidence for Grenvillian orogenesis? Journal of the Geological Society, v. 157, p. 1215–1225, doi:10.1144/jgs.157.6.1215.

Keller, C.B., Husson, J.M., Mitchell, R.N., Bottke, W.F., Gernon, T.M., Boehnke, P., Bell, E.A., Swanson-Hysell, N.L., and Peters, S.E., 2019, Neoproterozoic glacial origin of the Great Unconformity: Proceedings of the National Academy of Sciences, v. 116, p. 1136–1145, doi:10.1073/pnas.1804350116.

Kinnaird, T.C., Prave, A.R., Kirkland, C.L., Horstwood, M., Parrish, R., and Batchelor, A., 2009, The late Mesoproterozoic–early Neoproterozoic tectonostratigraphic evolution of NW Scotland: the Torridonian revisited: Journal of the Geological Society, v. 164, p. 541–551, doi:10.1144/0016-76492005-096.

Knoll, A.H., 1982, Microfossil-based biostratigraphy of the Precambrian Hecla Hoek sequence, Nordaustlandet, Svalbard: Geological Magazine, v. 119, p. 269–279, doi:10.1017/S001675680002608X.

Knoll, H., and Calder, S., 1983, Microbiotas of the late Precambrian Rysso Formation, Nordaustlandet, Svalbard: Paleontology, v. 26.

Knoll, A.H., Hayes, J.M., Kaufman, A.J., Swett, K., and Lambert, I.B., 1986, Secular variation in carbon isotope ratios from Upper Proterozoic successions of Svalbard and East Greenland: Nature, v. 321, p. 832–838, doi:10.1038/321832a0.

Knoll, A.H., and Swett, K., 1990, Carbonate deposition during the late Proterozoic Era: an example from Spitsbergen: American Journal of Science, v. 290-A, p. 104–132.

Knoll, H., and Swett, K., 1985, Micropaleontology of the late Proterozoic Veteranen Group, Spitsbergen: Palaeontology, v. 28, p. 23.

Knoll, A.H., Swett, K., and Mark, J., 1991, Paleobiology of a Neoproterozoic Tidal Flat/Lagoonal Complex: The Draken Conglomerate Formation, Spitsbergen: Journal of Paleontology, v. 65, p. 531–570.

Krabbendam, M., Bonsor, H., Horstwood, M.S.A., and Rivers, T., 2017, Tracking the evolution of the Grenvillian foreland basin: Constraints from sedimentology and detrital zircon and rutile in the Sleat and Torridon groups, Scotland: Precambrian Research, v. 295, p. 67–89, doi:10.1016/j.precamres.2017.04.027.

Kunzmann, M., Halverson, G.P., Scott, C., Minarik, W.G., and Wing, B.A., 2015, Geochemistry of Neoproterozoic black shales from Svalbard: Implications for oceanic redox conditions spanning Cryogenian glaciations: Chemical Geology, v. 417, p. 383–393, doi:10.1016/j.chemgeo.2015.10.022.

Li, Z.X. et al., 2008, Assembly, configuration, and break-up history of Rodinia: A synthesis: Precambrian Research, v. 160, p. 179–210, doi:10.1016/j.precamres.2007.04.021.

Li, X., and McCulloch, M.T., 1996, Secular variation in the Nd isotopic composition of Neoproterozoic sediments from the southern margin of the Yangtze Block: evidence for a Proterozoic continental collision in southeast China: Precambrian Research, v. 76, p. 67–76, doi:10.1016/0301-9268(95)00024-0.

Lorenz, H., Gee, D.G., Larionov, A.N., and Majka, J., 2012, The Grenville–Sveconorwegian orogen in the high Arctic: Geological Magazine, v. 149, p. 875–891, doi:10.1017/S0016756811001130.

Lu, W., Wörndle, S., Halverson, G.P., Zhou, X., Bekker, A., Rainbird, R.H., Hardisty, D.S., Lyons, T.W., and Lu, Z., 2017, Iodine proxy evidence for increased ocean oxygenation during the Bitter Springs Anomaly: Geochemical Perspectives Letters, p. 53–57, doi:10.7185/geochemlet.1746.

Macdonald, F.A., Schmitz, M.D., Crowley, J.L., Roots, C.F., Jones, D.S., Maloof, A.C., Strauss, J.V., Cohen, P.A., Johnston, D.T., and Schrag, D.P., 2010, Calibrating the Cryogenian: Science, v. 327, p. 1241–1243, doi:10.1126/science.1183325.

Macdonald, F.A., Schmitz, M.D., Strauss, J.V., Halverson, G.P., Gibson, T.M., Eyster, A., Cox, G., Mamrol, P., and Crowley, J.L., 2018, Cryogenian of Yukon: Precambrian Research, v. 319, p. 114–143, doi:10.1016/j.precamres.2017.08.015.

Macdonald, F.A., and Swanson-Hysell, N.L., 2023, The Franklin Large Igneous Province and Snowball Earth Initiation: Elements, v. 19, p. 296–301, doi:10.2138/gselements.19.5.296.

Macdonald, F.A., Swanson-Hysell, N.L., Park, Y., Lisiecki, L., and Jagoutz, O., 2019, Arc-continent collisions in the tropics set Earth's climate state: Science, p. eaav5300, doi:10.1126/science.aav5300.

MacLennan, S., Park, Y., Swanson-Hysell, N., Maloof, A., Schoene, B., Gebreslassie, M., Antilla, E., Tesema, T., Alene, M., and Haileab, B., 2018, The arc of the Snowball: U-Pb dates constrain the Islay anomaly and the initiation of the Sturtian glaciation: Geology, v. 46, p. 539–542, doi:10.1130/G40171.1.

Maliva, R.G., Knoll, A.H., and Simonson, B.M., 2005, Secular change in the Precambrian silica cycle: Insights from chert petrology: Geological Society of America Bulletin, v. 117, p. 835, doi:10.1130/B25555.1.

Maloney, K.M. et al., 2021, New multicellular marine macroalgae from the early Tonian of northwestern Canada: Geology, v. 49, p. 743–747, doi:10.1130/G48508.1.

Maloof, A.C., Halverson, G.P., Kirschvink, J.L., Schrag, D.P., Weiss, B.P., and Hoffman, P.F., 2006, Combined paleomagnetic, isotopic, and stratigraphic evidence for true polar wander from the Neoproterozoic Akademikerbreen Group, Svalbard, Norway: Geological Society of America Bulletin, p. 26.

McCulloch, M.T., and Wasserburg, G.J., 1978, Sm-Nd and Rb-Sr Chronology of Continental Crust Formation: Times of addition to continents of chemically fractionated mantle-derived materials are determined.: Science, v. 200, p. 1003–1011, doi:10.1126/science.200.4345.1003.

McLelland, J.M., Selleck, B.W., and Bickford, M.E., 2013, Tectonic Evolution of the Adirondack Mountains and Grenville Orogen Inliers within the USA: Geoscience Canada, v. 40, p. 318–352, doi:10.12789/geocanj.2013.40.022.

McLennan, S.M., 1989, Rare earth elements in sedimentary rocks: influence of provenance and sedimentary processes, *in* Lipin, B.R. and McKay, G.A. eds., Reviews in Mineralogy 21, Berlin, Boston: De Gruyter, p. 169–200.

McLennan, S.M., and Hemming, S., 1992, Samarium/neodymium elemental and isotopic systematics in sedimentary rocks: Geochimica et Cosmochimica Acta, v. 56, p. 887–898, doi:10.1016/0016-7037(92)90034-G.

McLennan, S., Hemming, S., and McDaniel, D., 1993, Geochemical approaches to sedimentation, provenance, and tectonics: Geological Society of America, v. Special Paper 284, p. 21–40.

McMahon, S., Anderson, R.P., Saupe, E.E., and Briggs, D.E.G., 2016, Experimental evidence that clay inhibits bacterial decomposers: Implications for preservation of organic fossils: Geology, v. 44, p. 867–870, doi:10.1130/G38454.1.

Menuge, J.F., 1988, The petrogenesis of massif anorthosites: a Nd and Sr isotopic investigation of the Proterozoic of Rogaland/Vest-Agder, SW Norway: Contributions to Mineralogy and Petrology, v. 98, p. 363–373, doi:10.1007/BF00375186.

Millikin, A.E.G., Strauss, J.V., Halverson, G.P., Bergmann, K.D., Tosca, N.J., and Rooney, A.D., 2022, Calibrating the Russøya excursion in Svalbard, Norway, and implications for Neoproterozoic chronology: Geology, v. 50, p. 506–510, doi:10.1130/G49593.1.

Mughal, S., Millikin, A.E.G., Zhang, T., Gibson, T.M., Rooney, A.D., Tosca, N.J., Bergmann, K.D., Strauss, J.V., and Anderson, R.P., 2025, The Svanbergfjellet Formation: eukaryotic life in a Tonian sea: Journal of the Geological Society, v. 182, doi:10.1144/jgs2024-083.

Nesbitt, H.W., and Young, G.M., 1982, Early Proterozoic climates and plate motions inferred from major element chemistry of lutites: Nature, v. 299, p. 715–717, doi:10.1038/299715a0.

Nesbitt, H.W., and Young, G.M., 1989, Formation and Diagenesis of Weathering Profiles: The Journal of Geology, v. 97, p. 129–147, doi:10.1086/629290.

Ohta, Y., 1985, Geochemistry of the late Proterozoic Kapp Hansteen igneous rocks of Nordaustlandet, Svalbard: Polar Research, v. 3, p. 69–92, doi:10.3402/polar.v3i1.6940.

Olierook, H.K.H., Barham, M., Kirkland, C.L., Hollis, J., and Vass, A., 2020, Zircon fingerprint of the Neoproterozoic North Atlantic Perspectives from East Greenland: Precambrian Research, v. 342, p. 105653, doi:10.1016/j.precamres.2020.105653.

Orr, P.J., Briggs, D.E.G., and Kearns, S.L., 1998, Cambrian Burgess Shale Animals Replicated in Clay Minerals: Science, v. 281, p. 1173–1175, doi:10.1126/science.281.5380.1173.

Park, Y. et al., 2020, The lead-up to the Sturtian Snowball Earth: Neoproterozoic chemostratigraphy time-calibrated by the Tambien Group of Ethiopia: GSA Bulletin, v. 132, p. 1119–1149, doi:10.1130/B35178.1.

Petrovich, R., 2001, Mechanisms of fossilization of the soft-bodied and lightly armored faunas of the Burgess Shale and of some other classical localities: American Journal of Science, v. 301, p. 683–726, doi:10.2475/ajs.301.8.683.

Pierrehumbert, R.T., 2004, High levels of atmospheric carbon dioxide necessary for the termination of global glaciation: Nature, v. 429, p. 646–649, doi:10.1038/nature02640.

Pin, C., and Zalduegui, J.S., 1997, Sequential separation of light rare-earth elements, thorium and uranium by miniaturized extraction chromatography: application to isotopic analyses of silicate rocks: Analytica Chimica Acta, v. 339, p. 79–89.

Pu, J.P., Macdonald, F.A., Schmitz, M.D., Rainbird, R.H., Bleeker, W., Peak, B.A., Flowers, R.M., Hoffman, P.F., Rioux, M., and Hamilton, M.A., 2022, Emplacement of the Franklin large igneous province and initiation of the Sturtian Snowball Earth: Science Advances, v. 8, p. eadc9430, doi:10.1126/sciadv.adc9430.

Rainbird, R., Cawood, P., and Gehrels, G., 2011, The Great Grenvillian Sedimentation Episode: Record of Supercontinent Rodinia’s assembly, *in* Busby, C. and Azor, A. eds., Tectonics of Sedimentary Basins, Wiley, p. 583–601, doi:10.1002/9781444347166.ch29.

Rainbird, R.H., McNicoll, V.J., Thériault, R.J., Heaman, L.M., Abbott, J.G., Long, D.G.F., and Thorkelson, D.J., 1997, Pan-Continental River System Draining Grenville Orogen Recorded by U-Pb and Sm-Nd Geochronology of Neoproterozoic Quartzarenites and

Mudrocks, Northwestern Canada: The Journal of Geology, v. 105, p. 1–17, doi:10.2307/30079882.

Rainbird, R.H., Rayner, N.M., Hadlari, T., Heaman, L.M., Ielpi, A., Turner, E.C., and MacNaughton, R.B., 2017, Zircon provenance data record the lateral extent of pancontinental, early Neoproterozoic rivers and erosional unroofing history of the Grenville orogen: GSA Bulletin, v. 129, p. 1408–1423, doi:10.1130/B31695.1.

Reahl, J.N., Cantine, M.D., Wilcots, J., Mackey, T.J., and Bergmann, K.D., 2021, Meta-analysis of Cryogenian through modern quartz microtextures reveals sediment transport histories: Journal of Sedimentary Research, v. 91, p. 929–944, doi:10.2110/jsr.2020.151.

Riedman, L.A., Porter, S.M., and Calver, C.R., 2018, Vase-shaped microfossil biostratigraphy with new data from Tasmania, Svalbard, Greenland, Sweden and the Yukon: Precambrian Research, v. 319, p. 19–36, doi:10.1016/j.precamres.2017.09.019.

Roest-Ellis, S., Richardson, J.A., Phillips, B.L., Mehra, A., Webb, S.M., Cohen, P.A., Strauss, J.V., and Tosca, N.J., 2023, Tonian Carbonates Record Phosphate-Rich Shallow Seas: Geochemistry, Geophysics, Geosystems, v. 24, p. e2023GC010974, doi:10.1029/2023GC010974.

Rooney, A.D., Austermann, J., Smith, E.F., Li, Y., Selby, D., Dehler, C.M., Schmitz, M.D., Karlstrom, K.E., and Macdonald, F.A., 2018, Coupled Re-Os and U-Pb geochronology of the Tonian Chuar Group, Grand Canyon: GSA Bulletin, v. 130, p. 1085–1098, doi:10.1130/B31768.1.

Rooney, A.D., Macdonald, F.A., Strauss, J.V., Dudas, F.O., Hallmann, C., and Selby, D., 2014, Re-Os geochronology and coupled Os-Sr isotope constraints on the Sturtian snowball Earth: Proceedings of the National Academy of Sciences, v. 111, p. 51–56, doi:10.1073/pnas.1317266110.

Rooney, A.D., Strauss, J.V., Brandon, A.D., and Macdonald, F.A., 2015, A Cryogenian chronology: Two long-lasting synchronous Neoproterozoic glaciations: Geology, v. 43, p. 459–462, doi:10.1130/G36511.1.

Rooney, A.D., Yang, C., Condon, D.J., Zhu, M., and Macdonald, F.A., 2020, U-Pb and Re-Os geochronology tracks stratigraphic condensation in the Sturtian snowball Earth aftermath: Geology, v. 48, p. 625–629, doi:10.1130/G47246.1.

Rose, C.V., Maloof, A.C., Schoene, B., Ewing, R.C., Linnemann, U., Hofmann, M., and Cottle, J.M., 2013, The End-Cryogenian Glaciation of South Australia: Geoscience Canada, v. 40, p. 256–293, doi:10.12789/geocanj.2013.40.019.

Rudnick, R.L., and Gao, S., 2003, 3.01 Composition of the Continental Crust, *in* Holland, H.D. and Turekian, K.K. eds., Treatise on Geochemistry, Elsevier, v. 3, p. 1–64.

Sandelin, S., Tebenkov, A.M., and Gee, D.G., 2001, The stratigraphy of the lower part of the Neoproterozoic Murchisonfjorden Supergroup in Nordaustlandet, Svalbard: GFF, v. 123, p. 113–127, doi:10.1080/11035890101232113.

Schärer, U., Wilmart, E., and Duchesne, J.-C., 1996, The short duration and anorogenic character of anorthosite magmatism: U-Pb dating of the Rogaland complex, Norway: Earth and Planetary Science Letters, v. 139, p. 335–350, doi:10.1016/0012-821X(96)00033-7.

Shellnutt, J., 2004, Petrogenesis of the 723 Ma Coronation sills, Amundsen basin, Arctic Canada: implications for the break-up of Rodinia: Precambrian Research, v. 129, p. 309–324, doi:10.1016/j.precamres.2003.10.006.

Shirey, S.B., and Hanson, G.N., 1986, Mantle heterogeneity and crustal recycling in Archean granite-greenstone belts: Evidence from Nd isotopes and trace elements in the Rainy Lake area, Superior Province, Ontario, Canada: Geochimica et Cosmochimica Acta, v. 50, p. 2631–2651, doi:10.1016/0016-7037(86)90215-2.

Shirey, S.B., Kamber, B.S., Whitehouse, M.J., Mueller, P.A., and Basu, A.R., 2008, A review of the isotopic and trace element evidence for mantle and crustal processes in the Hadean and Archean: Implications for the onset of plate tectonic subduction, *in* Special Paper 440: When Did Plate Tectonics Begin on Planet Earth?, Geological Society of America, v. 440, p. 1–29, doi:10.1130/2008.2440(01).

Slagstad, T. et al., 2018, Magma-driven, high-grade metamorphism in the Sveconorwegian Province, southwest Norway, during the terminal stages of Fennoscandian Shield evolution: Geosphere, v. 14, p. 861–882, doi:10.1130/GES01565.1.

Slagstad, T., Roberts, N.M.W., Marker, M., Røhr, T.S., and Schiellerup, H., 2013, A non-collisional, accretionary Sveconorwegian orogen: Terra Nova, v. 25, p. 30–37, doi:10.1111/ter.12001.

Sønderholm, M., Frederiksen, K.S., Smith, M.P., and Tirsgaard, H., 2008, Neoproterozoic sedimentary basins with glacigenic deposits of the East Greenland Caledonides, *in* Higgins, A.K., Gilotti, J.A., and Smith, M.P. eds., Memoir 202: The Greenland Caledonides: Evolution of the Northeast Margin of Laurentia,.

Sperling, E.A., Halverson, G.P., Knoll, A.H., Macdonald, F.A., and Johnston, D.T., 2013, A basin redox transect at the dawn of animal life: Earth and Planetary Science Letters, v. 371–372, p. 143–155, doi:10.1016/j.epsl.2013.04.003.

Strauss, J.V., Rooney, A.D., Macdonald, F.A., Brandon, A.D., and Knoll, A.H., 2014, 740 Ma vase-shaped microfossils from Yukon, Canada: Implications for Neoproterozoic chronology and biostratigraphy: Geology, v. 42, p. 659–662, doi:10.1130/G35736.1.

Sundell, K.E., and Macdonald, F.A., 2022, The tectonic context of hafnium isotopes in zircon: Earth and Planetary Science Letters, v. 584, p. 117426, doi:10.1016/j.epsl.2022.117426.

Swanson-Hysell, N.L., Maloof, A.C., Condon, D.J., Jenkin, G.R.T., Alene, M., Tremblay, M.M., Tesema, T., Rooney, A.D., and Haileab, B., 2015, Stratigraphy and geochronology of the Tambien Group, Ethiopia: Evidence for globally synchronous carbon isotope change in the Neoproterozoic: Geology, v. 43, p. 323–326, doi:10.1130/G36347.1.

Swett, K., and Knoll, A.H., 1985, Stromatolitic bioherms and microphytolites from the late Proterozoic Draken conglomerate formation, Spitsbergen: Precambrian Research, v. 28, p. 327–347, doi:10.1016/0301-9268(85)90037-3.

Taylor, S.R., and McLennan, S.M., 1985, The continental crust: its composition and evolution: Oxford ; Boston : Blackwell Scientific ; Palo Alto, Calif. : Distributors, USA and Canada, Blackwell Scientific, 312 p.

Tosca, N.J., Johnston, D.T., Mushegian, A., Rothman, D.H., Summons, R.E., and Knoll, A.H., 2010, Clay mineralogy, organic carbon burial, and redox evolution in Proterozoic oceans: Geochimica et Cosmochimica Acta, v. 74, p. 1579–1592, doi:10.1016/j.gca.2009.12.001.

Tosca, N.J., Macdonald, F.A., Strauss, J.V., Johnston, D.T., and Knoll, A.H., 2011, Sedimentary talc in Neoproterozoic carbonate successions: Earth and Planetary Science Letters, v. 306, p. 11–22, doi:10.1016/j.epsl.2011.03.041.

Turner, S., Foden, J., Sandiford, M., and Bruce, D., 1993, Sm-Nd isotopic evidence for the provenance of sediments from the Adelaide Fold Belt and southeastern Australia with implications for episodic crustal addition: Geochimica et Cosmochimica Acta, v. 57, p. 1837–1856, doi:10.1016/0016-7037(93)90116-E.

Van Acken, D., Thomson, D., Rainbird, R.H., and Creaser, R.A., 2013, Constraining the depositional history of the Neoproterozoic Shaler Supergroup, Amundsen Basin, NW Canada: Rhenium-osmium dating of black shales from the Wynniatt and Boot Inlet Formations: Precambrian Research, v. 236, p. 124–131, doi:10.1016/j.precamres.2013.07.012.

Vander Auwera, J., Bogaerts, M., Liégeois, J.-P., Demaiffe, D., Wilmart, E., Bolle, O., and Duchesne, J.C., 2003, Derivation of the 1.0–0.9 Ga ferro-potassic A-type granitoids of southern Norway by extreme differentiation from basic magmas: Precambrian Research, v. 124, p. 107–148, doi:10.1016/S0301-9268(03)00084-6.

Vautour, S., and Dickin, A., 2019, Nd isotope mapping of a Pinwarian-age composite arc belt in the Quebecia terrane of the central Grenville Province, Canada: Precambrian Research, v. 332, p. 105409, doi:10.1016/j.precamres.2019.105409.

Wade, B.P., Hand, M., and Barovich, K.M., 2005, Nd isotopic and geochemical constraints on provenance of sedimentary rocks in the eastern Officer Basin, Australia: implications for the duration of the intracratonic Petermann Orogeny: Journal of the Geological Society, London, v. 163, p. 513–530, doi:10.1144/0016-764904-001.

Wala, V.T., Ziemniak, G., Majka, J., Faehnrich, K., McClelland, W.C., Meyer, E.E., Manecki, M., Bazarnik, J., and Strauss, J.V., 2021, Neoproterozoic stratigraphy of the

Southwestern Basement Province, Svalbard (Norway): Constraints on the Proterozoic-Paleozoic evolution of the North Atlantic-Arctic Caledonides: Precambrian Research, v. 358, p. 106138, doi:10.1016/j.precamres.2021.106138.

Wang, P., Du, Y., Yu, W., Algeo, T.J., Zhou, Q., Xu, Y., Qi, L., Yuan, L., and Pan, W., 2020, The chemical index of alteration (CIA) as a proxy for climate change during glacial-interglacial transitions in Earth history: Earth-Science Reviews, v. 201, p. 103032, doi:10.1016/j.earscirev.2019.103032.

Wang, X.-C., Li, Z.-X., Li, X.-H., Li, Q.-L., and Zhang, Q.-R., 2011, Geochemical and Hf–Nd isotope data of Nanhua rift sedimentary and volcaniclastic rocks indicate a Neoproterozoic continental flood basalt provenance: Lithos, v. 127, p. 427–440, doi:10.1016/j.lithos.2011.09.020.

Watt, G.R., and Thrane, K., 2001, Early Neoproterozoic events in East Greenland: Precambrian Research, v. 110, p. 165–184, doi:10.1016/S0301-9268(01)00186-3.

Welin, E., 1994, Isotopic investigations of Proterozoic igneous rocks in south-western Sweden: GFF, v. 116, p. 75–86, doi:10.1080/11035899409546162.

Whitmeyer, S.J., and Karlstrom, K.E., 2007, Tectonic model for the Proterozoic growth of North America: Geosphere, v. 3, p. 220–259, doi:10.1130/GES00055.1.

Wilson, C.B., 1958, The Lower Middle Hecla Hoek Rocks of Ny Friesland, Spitsbergen: Geological Magazine, v. 95, p. 305–327, doi:10.1017/S0016756800062865.

Wilson, C.B., 1961, The Upper Middle Hecla Hoek Rocks of Ny Friesland, Spitsbergen: Geological Magazine, v. 98, p. 89–116, doi:10.1017/S0016756800060325.

Wilson, L.A., and Butterfield, N.J., 2014, Sediment effects on the Preservation of Burgess Shale-Type compression fossils: PALAIOS, v. 29, p. 145–154, doi:10.2110/palo.2013.075.

Woltz, C.R., Anderson, R.P., Tosca, N.J., and Porter, S.M., 2023, The role of clay minerals in the preservation of Precambrian organic-walled microfossils: Geobiology, v. 21, p. 708–724, doi:10.1111/gbi.12573.

Wörndle, S., Crockford, P.W., Kunzmann, M., Bui, T.H., and Halverson, G.P., 2019, Linking the Bitter Springs carbon isotope anomaly and early Neoproterozoic oxygenation through I/[Ca + Mg] ratios: Chemical Geology, v. 524, p. 119–135, doi:10.1016/j.chemgeo.2019.06.015.

Xiao, S., and Tang, Q., 2018, After the boring billion and before the freezing millions: evolutionary patterns and innovations in the Tonian Period (T. W. Lyons, M. L. Droser, K. V. Lau, & S. M. Porter, Eds.): Emerging Topics in Life Sciences, v. 2, p. 161–171, doi:10.1042/ETLS20170165.

Yang, Y., Zhang, H., Chu, Z., Xie, L., and Wu, F., 2010, Combined chemical separation of Lu, Hf, Rb, Sr, Sm and Nd from a single rock digest and precise and accurate isotope determinations of Lu–Hf, Rb–Sr and Sm–Nd isotope systems using Multi-Collector ICP-MS and TIMS: International Journal of Mass Spectrometry, v. 290, p. 120–126.

Zhang, T., Keller, C.B., Hoggard, M.J., Rooney, A.D., Halverson, G.P., Bergmann, K.D., Crowley, J.L., and Strauss, J.V., 2023, A Bayesian framework for subsidence modeling in sedimentary basins: A case study of the Tonian Akademikerbreen Group of Svalbard, Norway: Earth and Planetary Science Letters, v. 620, p. 118317, doi:10.1016/j.epsl.2023.118317.

Zhao, J.X., McCulloch, M.T., and Bennett, V.C., 1992, Sm-Nd and U-Pb zircon isotopic constraints on the provenance of sediments from the Amadeus Basin, central Australia: Evidence for REE fractionation: Geochimica et Cosmochimica Acta, v. 56, p. 921–940, doi:10.1016/0016-7037(92)90037-J.

Zhou, Y., Pogge von Strandmann, P.A.E., Zhu, M., Ling, H., Manning, C., Li, D., He, T., and Shields, G.A., 2020, Reconstructing Tonian seawater $^{87}Sr/^{86}Sr$ using calcite microspar: Geology, v. 48, p. 462–467, doi:10.1130/G46756.1.

FIGURE AND TABLE CAPTIONS

Table 1. Sample subsets of the Lomfjorden and lower Hinlopenstretet supergroup sedimentary rocks and basement units of the Brennevinsfjorden and Kapp Hansteen groups used to filter geochemical data (see Supplementary Material for further details on subsets).

Figure 1. (A) Generalized stratigraphic column of the Lomfjorden and lower Hinlopenstretet supergroups and underlying units, showing existing age constraints from: 1. Lorenz et al. (2012), 2. Johansson et al. (1999), 3. Zhang et al. (2023), and 4. Millikin et al. (2022). Mpz.—Mesoproterozoic; Cr.—Cryogenian; Ed.—Ediacaran; Sgp.—Supergroup; Bsmt.—Basement; Brenn.—Brennevinsfjorden; Gp.—Group; Fm.—Formation; mb.—member; l.—lower; u.—upper; ls.—limestone; al.—algal; dol.—dolomite; Dart.—Dartboard; Pet.—Petrovbreen; Mac.—Macdonaldryggen; metased.—metasedimentary; DZ—detrital zircon; max. depo.—maximum depositional; (B) Generalized geologic map of the Eastern Province of northeastern Svalbard (location shown on inset) showing sample locations referenced in text (red numbers). LYR—Longyearbyen; Npz.—Neoproterozoic; ESZ—Eolussletta Shear Zone; LFZ—Lomfjorden Fault Zone.

Figure 2. (A) Plot of Ca/Al (molar proportions) vs. carbonate abundance (% whole rock) for mudrock samples with both geochemical and mineralogical data. The gray box denotes the area enlarged in panel (B). Samples are plotted by subset, used to filter geochemical data (see Table 1).

Figure 3. Plots of Rare Earth Elements (REEs) normalized to chondritic values, including post-Archean average shale (PAAS) for reference (Taylor and McLennan, 1985). Samples are plotted by subset, used to filter geochemical data, as discussed in the text and Table 1: (A) Carbonate

samples; (B) Mudrock samples with Ca/Al >1 and Ca/Al between 0.3 and 1; (C) "Fluorapatite" subset mudrocks characterized by middle REE (MREE) enrichment and samples with MREE depletion ("MREE Depleted" subset), possibly related to modern weathering; and (D) Mudrock samples with Ca/Al < 0.3 plotted with data for the Kapp Hansteen Group from Johansson et al. (1999) and this study. Missing datapoints indicate that concentration was below the analytical detection limit.

Figure 4. Plots of Ca/Al, a proxy for carbonate content, against various geochemical provenance and weathering proxies, including: (A) ε_{Nd} at time of deposition ($\varepsilon_{Nd(T)}$); (B) Th/Sc; (C) Eu anomaly (Eu_n/Eu_n^*); and (D) Chemical Index of Alteration (CIA). Mudrock samples are plotted by subset, used to filter geochemical data (Table 1).

Figure 5. Plots of Al_2O_3 (wt %) against major oxides with mudrock samples differentiated by subset, used to filter geochemical data (Table 1).

Figure 6. Major oxide ternary plots, including ACNK in (A) and (C) and ACNKFM in (B) and (D), showing mineral compositions for reference (yellow squares). Chemical index of alteration (CIA) corresponds with position along the molar proportion of Al_2O_3 axis in the ACNK ternary. In (A) and (B), mudrock samples from the "provenance and weathering subset" are differentiated by stratigraphic unit and fields for the underlying Kapp Hansteen Group are shown for reference (Ohta, 1985; Johansson et al., 1999; this study). Note that the Algal Dolomite member is plotted separately from the rest of the Svanbergfjellet Formation. In (C) and (D) mudrock samples with high Ca/Al ratios are differentiated from samples of the "provenance and weathering subset", and

carbonate samples are plotted for reference. Fm.—Formation; Mbr.—Member. Molar proportions of oxides were used to calculate ternary position (see Supplementary Material for details on correction of CaO for carbonate content (CaO^*)). Compositions of Post-Archean average shale (PAAS; Taylor and McLennan, 1985) and upper continental crust (UCC; Rudnick and Gao, 2003) are shown for reference.

Figure 7. Plots of geochemical and mineralogical data from mudrocks of the Lomfjorden and lower Hinlopenstretet supergroups against composite stratigraphic height, including (A) depositional chemical index of alteration (CIA_{paleo}), (B) Kaolinite/Clay Subtotal, (C) Th/Sc, (D) Eu anomaly (Eu_n/Eu_n^*), (E) Ti/Al, and (F) ε_{Nd} at the time of deposition ($\varepsilon_{Nd(T)}$). Data are differentiated by subset, used for filtering geochemical data (see Table 1). Data from the underlying Kapp Hansteen Group (Johansson et al., 1999; this study), Wilsonbreen diamictite (Cox et al., 2016b) and carbonate samples (this study) are plotted for comparison where available. Arrows in panel (C) indicate data out of the range of the plot. Bren.—Brennevinsfjorden; K.H.—Kapp Hansteen; Kort.—Kortbreen; King.—Kingbreen; Glas.—Glasgowbreen; Ox.—Oxfordbreen; Grus.—Grusdievbreen; Svan.—Svanbergfjellet; Drak.—Draken; Elbo.—Elbobreen; Wils.—Wilsonbreen; Draco.—Dracoisen; Polaris.—Polarisbreen; Hinlopen.—Hinlopenstretet; Sgp.—Supergroup; Gp.—Group; Fm.—Formation.

Figure 8.0 Plots of clay mineral abundance in mudrock samples from the Lomfjorden and lower Hinlopenstretet supergroups, including (A) muscovite/illite/montmorillonite; (B) kaolinite; (C) Fe chlorite/berthierine; (D) Mg chlorite; (E) smectite; and (F) the total abundance of clays. Samples are differentiated by subset, used for filtering geochemical data (see Table 1). Bren.—

Brennevinsfjorden; K.H.—Kapp Hansteen; Kort.—Kortbreen; King.—Kingbreen; Glas.—Glasgowbreen; Ox.—Oxfordbreen; Grus.—Grusdievbreen; Svan.—Svanbergfjellet; Drak.—Draken; Elbo.—Elbobreen; Wils.—Wilsonbreen; Draco.—Dracoisen; Polaris.—Polarisbreen; Hinlopen.—Hinlopenstretet; Sgp.—Supergroup; Gp.—Group; Fm.—Formation.

Figure 9. Box plots of geochemical metrics from mudrock and diamictite samples of the Lomfjorden and lower Hinlopenstretet supergroups organized by stratigraphic unit, including (A) Th/Sc, (B) Eu anomaly (Eu_n/Eu_n^*), (C) depositional chemical index of alteration (CIA_{paleo}), and (D) ε_{Nd} at time of deposition ($\varepsilon_{Nd(T)}$). Only data from the "provenance and weathering subset" are included in plots A–C, while data from all subsets are included in panel D (see Table 1 for explanation of subsets). Data from the Brennevinsfjorden and Kapp Hansteen groups are plotted for comparison (Ohta, 1985; Johansson et al., 1999; this study). Numbers above each boxplot indicate the number of samples included. Grey dots represent statistical outliers and red dots represent means. Gp.—Group; Fm.—Formation; Mbr.—Member, KH—Kapp Hansteen; Avg.—Average; Max.—Maximum; M—Marinoan.

Figure 10. Plots of trace elements used to differentiate tectonic setting in mudrocks. (A) Ternary plot of Th, Sc and Zr/10 with fields for tectonic settings from Bhatia and Crook (1986). OIA—ocean island arc; CIA—continental island arc; ACM—active continental margin; PM— passive margin. (B) Plot of La/Th against Hf with fields for different tectonic settings from Floyd and Leveridge (1987). Samples from the "provenance and weathering subset" are differentiated by stratigraphic unit while mudrocks with Ca/Al > 0.3 are plotted by subset (see Table 1 for explanation of subsets). Note that the Algal Dolomite member is plotted separately from the rest

of the Svanbergfjellet Formation. Arrow in panel (B) indicates data out of the range of the plot. Compositions of Post-Archean average shale (PAAS; Taylor and McLennan, 1985) and upper continental crust (UCC; Rudnick and Gao, 2003) are shown for reference. Fm.—Formation; Mb.—Member.

Figure 11. (A) Plot of ε_{Nd} at time of deposition ($\varepsilon_{Nd(T)}$) against sample age for Lomfjorden and lower Hinlopenstretet supergroup mudrocks and diamictites. Underlying units (Brennevinsfjorden and Kapp Hansteen groups) and East Greenland crystalline basement fields are plotted for reference (Kalsbeek et al., 1993; Johansson et al., 1999; this study). M.—Marinoan. (B) Plot of $\varepsilon_{Nd(T)}$ against Ca/Al where available. Dotted lines mark the Ca/Al = 0.3 and Ca/Al = 1 cut-offs used in mudrock sample filtering (see Figure 2). Note the logarithmic scale on the x-axis. Mbr.—Member; Fm.—Formation; Gp.—Group.

Figure 12. Filtered Sr isotope data from this study plotted along with the compilation of Chen et al. (2022) and data from Fairchild et al. (2016). M—Marinoan.

Figure 13. Plots of Th/Sc against ε_{Nd} at time of deposition ($\varepsilon_{Nd(T)}$) for Lomfjorden and lower Hinlopenstretet supergroup mudrocks after McLennan et al. (1993). In (A) mudrocks are differentiated by filtering subset (see Table 1) and in (B) they are colored by Zr/Ti. Data from the underlying Brennevinsfjorden (this study) and Kapp Hansteen groups (Johansson et al., 1999; this study), both with $\varepsilon_{Nd(T)}$ calculated at 800 Ma, are shown for reference. An estimate of Neoproterozoic juvenile material of mafic (mid-ocean ridge basalt—MORB) and intermediate

composition (Arc andesite) are shown using Th/Sc from McLennan et al. (1993) and $\varepsilon_{Nd(T)}$ from Shirey et al. (2008). Gp.—Group.

Figure 14. Plots of f_{SmNd} (present day) against $\varepsilon_{Nd(T)}$ (calculated for the sample's depositional age) for Lomfjorden and lower Hinlopenstretet supergroup mudrocks and diamictites after Shirey and Hanson (1986). Data are differentiated by filtering subset (A and B), described in the text and Table 1, and stratigraphic unit (C). Samples are plotted with fields for the Grenville (sources are listed in Table DR8) and Sveconorwegian provinces (Bolle et al., 2003; Granseth et al., 2020) in (A) and potential local sources in (B), including the underlying Kapp Hansteen Group (Johansson et al., 1999; this study) and East Greenland basement (Kalsbeek et al., 1993). $\varepsilon_{Nd(T)}$ of potential source units were calculated for the time spanning deposition of the Lomfjorden and lower Hinlopenstretet supergroups (914 and 630 Ma). An estimate of Neoproterozoic juvenile mafic material (mid-ocean ridge basalt—MORB) is shown using f_{SmNd} from McLennan et al. (1993) and $\varepsilon_{Nd(T)}$ from Shirey et al. (2008). Mbr.—Member; Fm.—Formation; Gp.—Group.

Figure 15. Plots of radiogenic isotopes used to investigate weathering and sediment provenance throughout the Neoproterozoic, including Nd isotope data from (A) South China, (B) Australia, (C) Laurentia, and (D) Svalbard; the global Sr isotope curve (E); and a compilation of global initial Os (Os*i*) data (F). Blue bars show the timing of the Sturtian and Marinoan Snowball Earth events. Nd isotope data from detrital siliciclastic units are shown in blue circles while data from iron formations are plotted as red squares. Data were originally compiled by Cox et al. (2016b) and age assignments have been updated where necessary (see Table DR9 for data and source). Nd isotope

data for each area are plotted with local basement and/or interpreted sources, large igneous province arrays (brown), and the mantle evolution curve (black). Data sources for the Nd isotope source fields and Neoproterozoic Sr and Os isotope data can be found in the Supplementary Material. E—East; KH—Kapp Hansteen; Bsmt.—Basement; Gp—Group; Lit—literature; Avg.—Average.

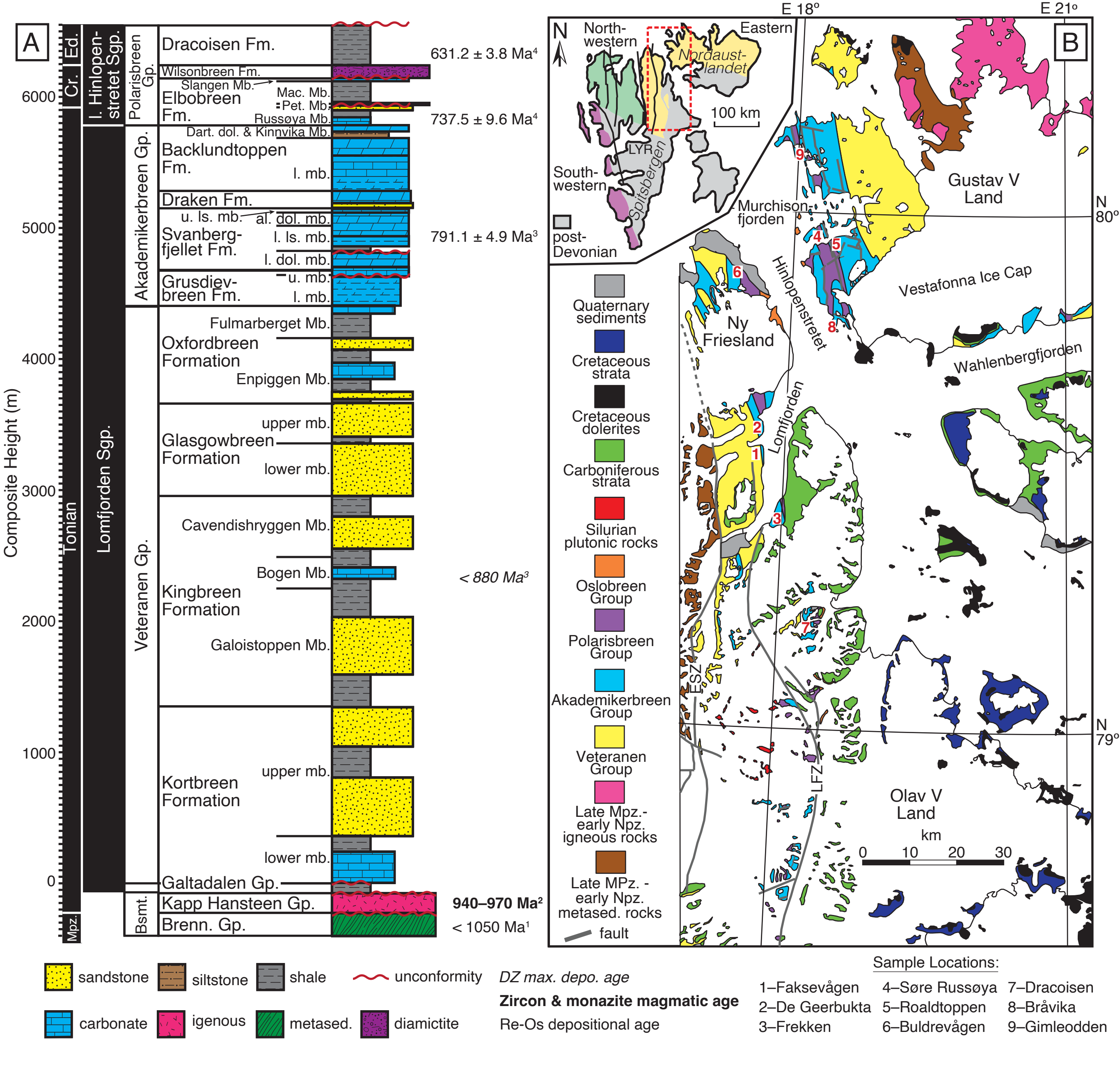

Millikin, Figure 1

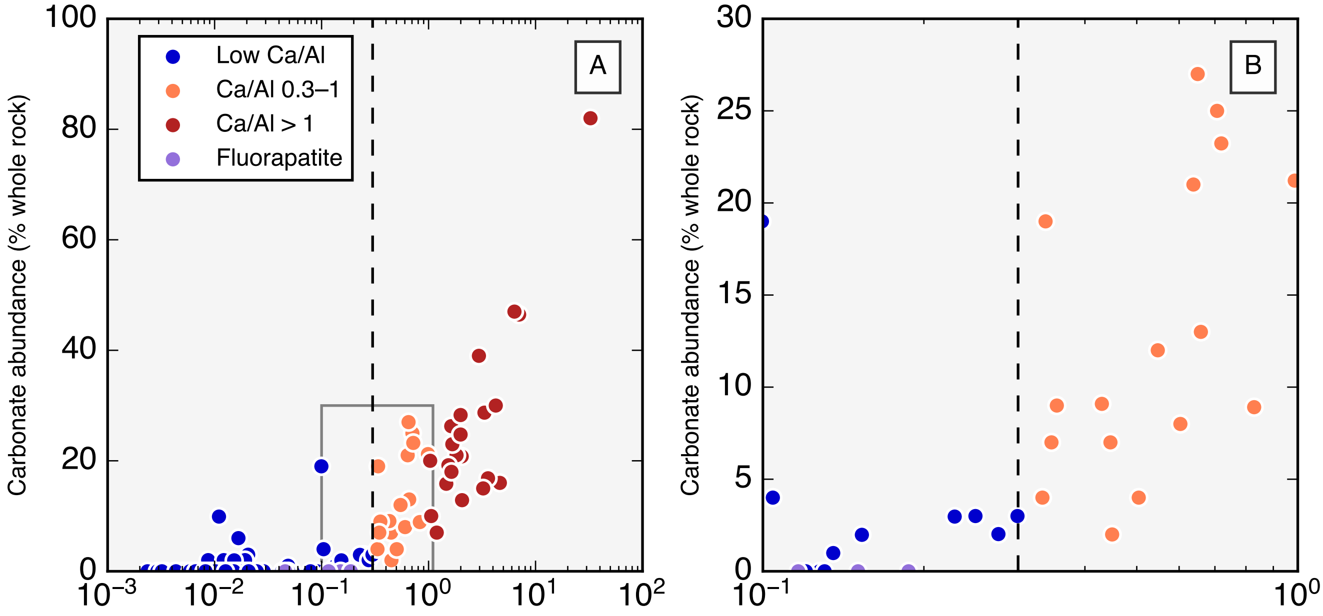

Millikin, Figure 2

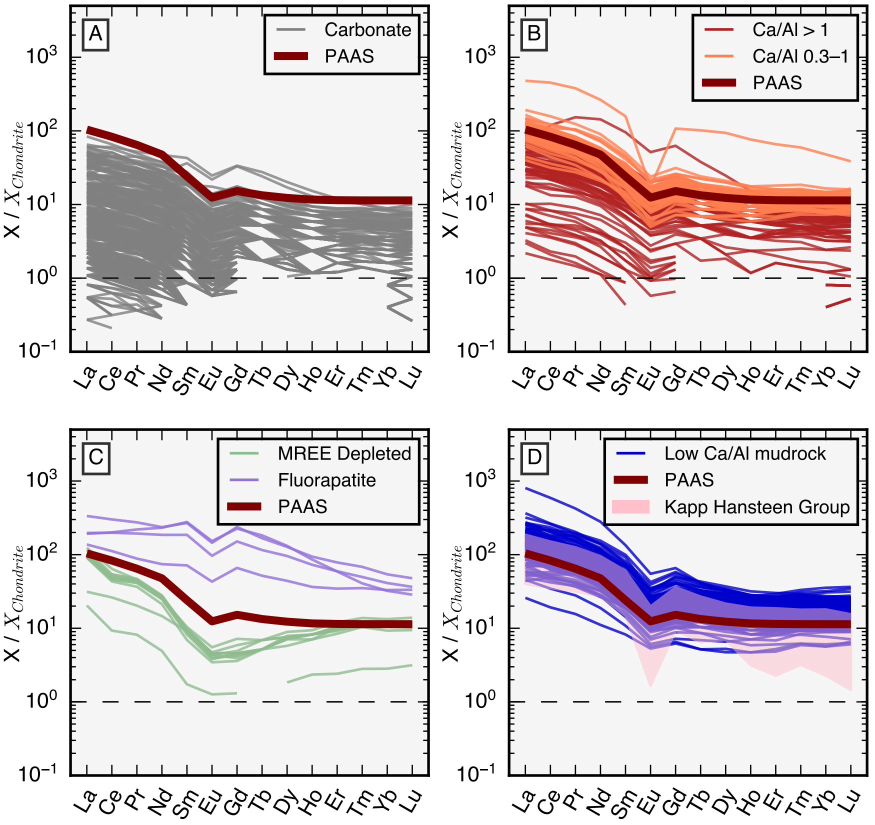

Millikin, Figure 3

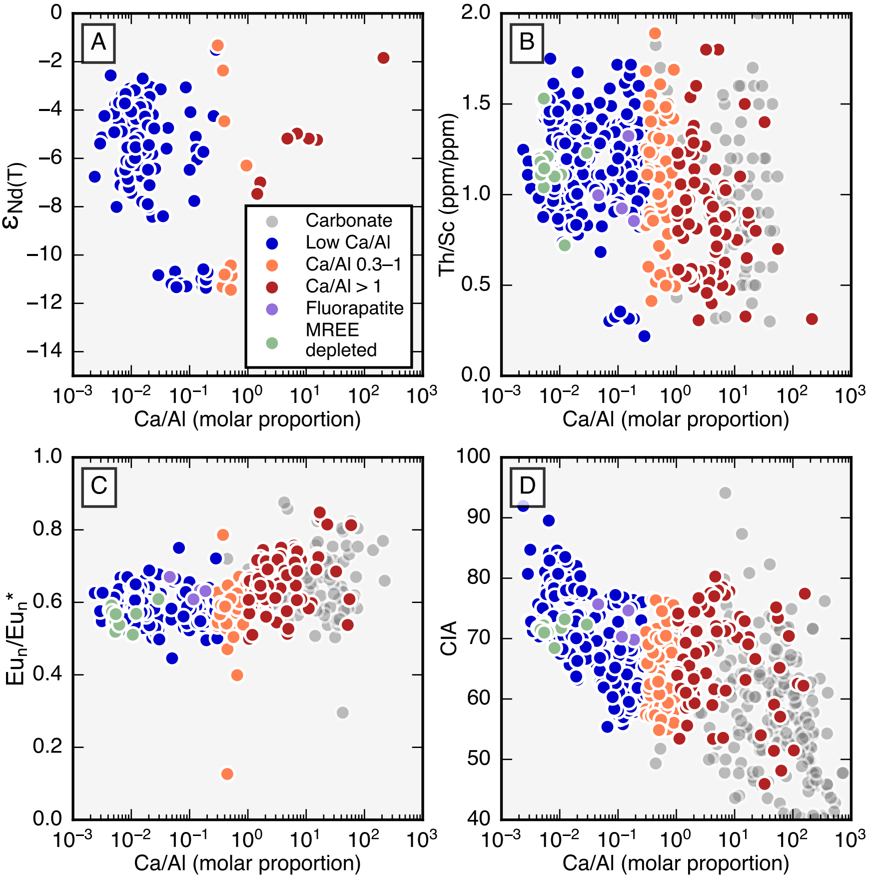

Millikin, Figure 4

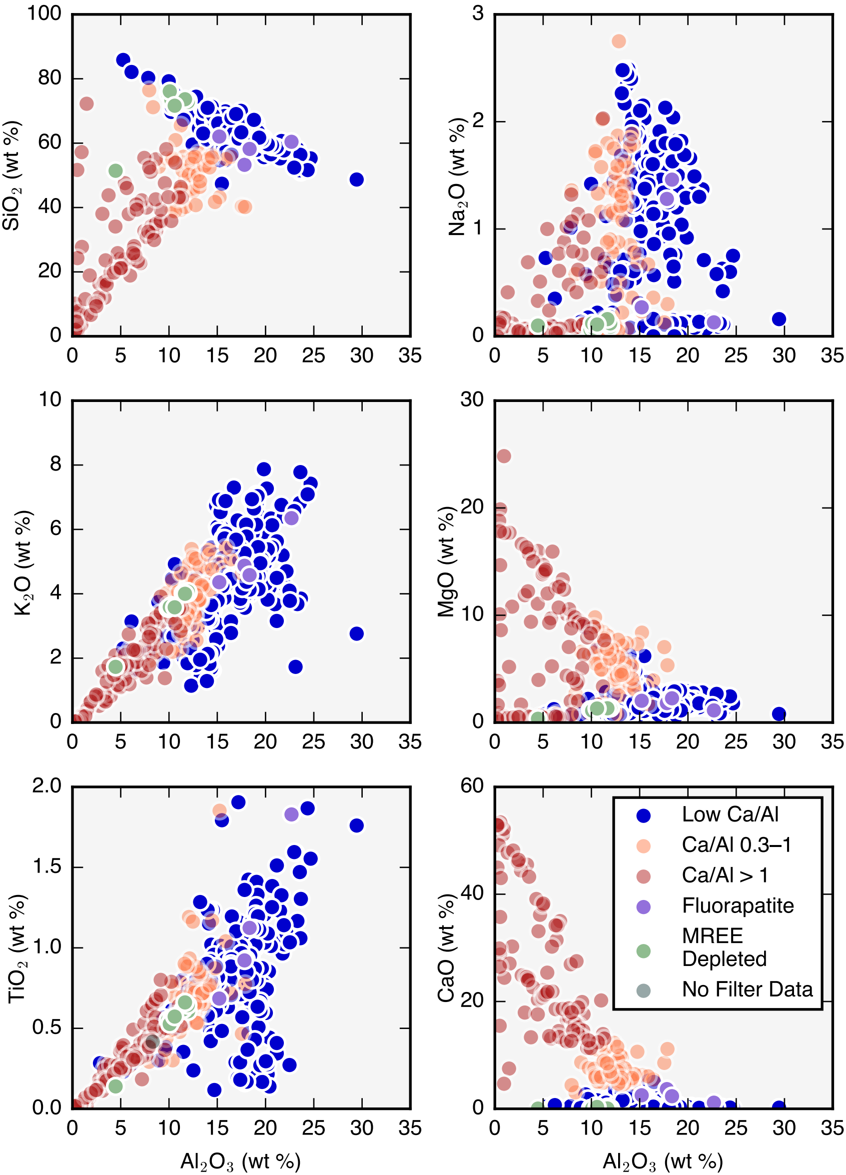

Millikin, Figure 5

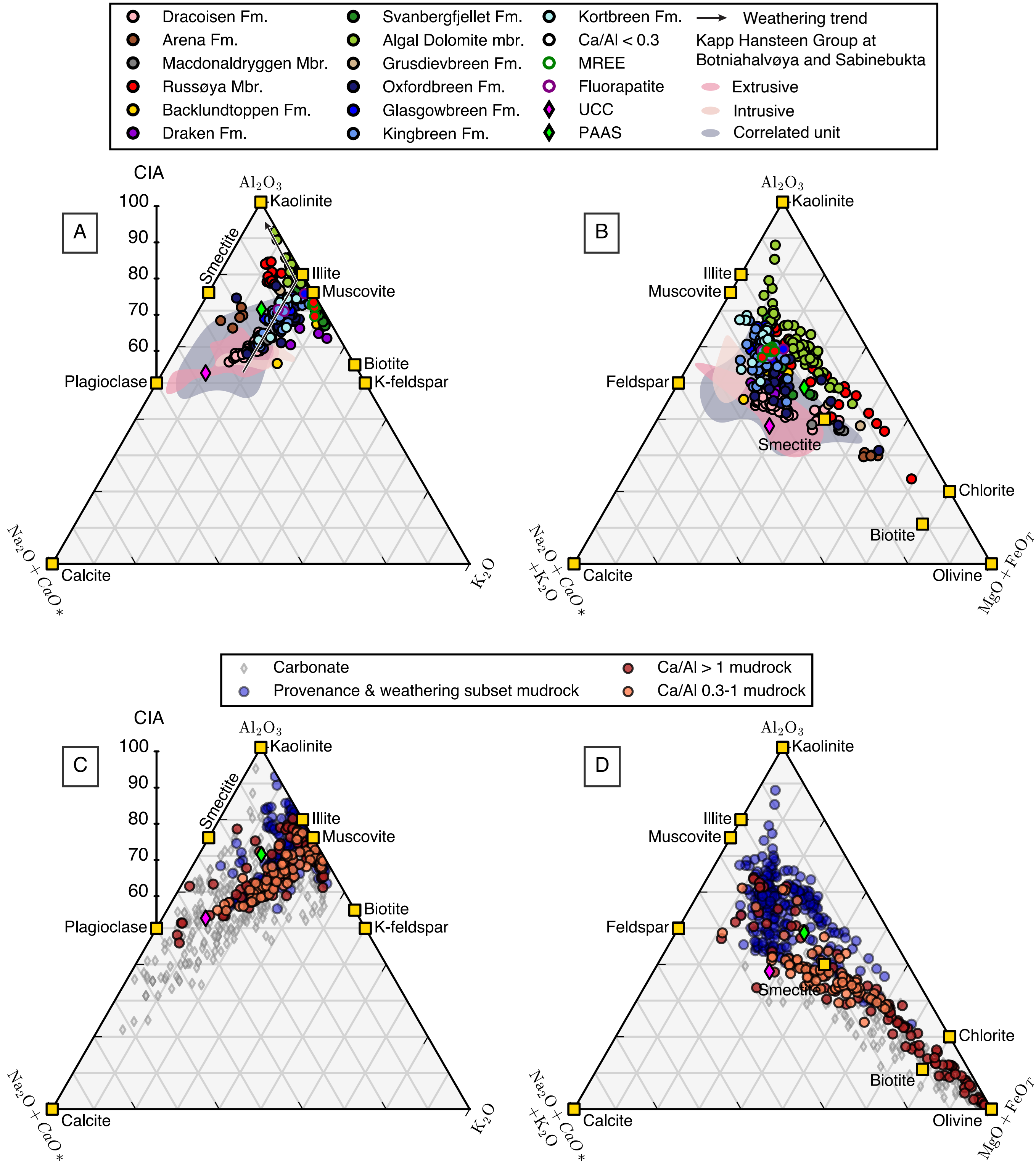

Millikin, Figure 5

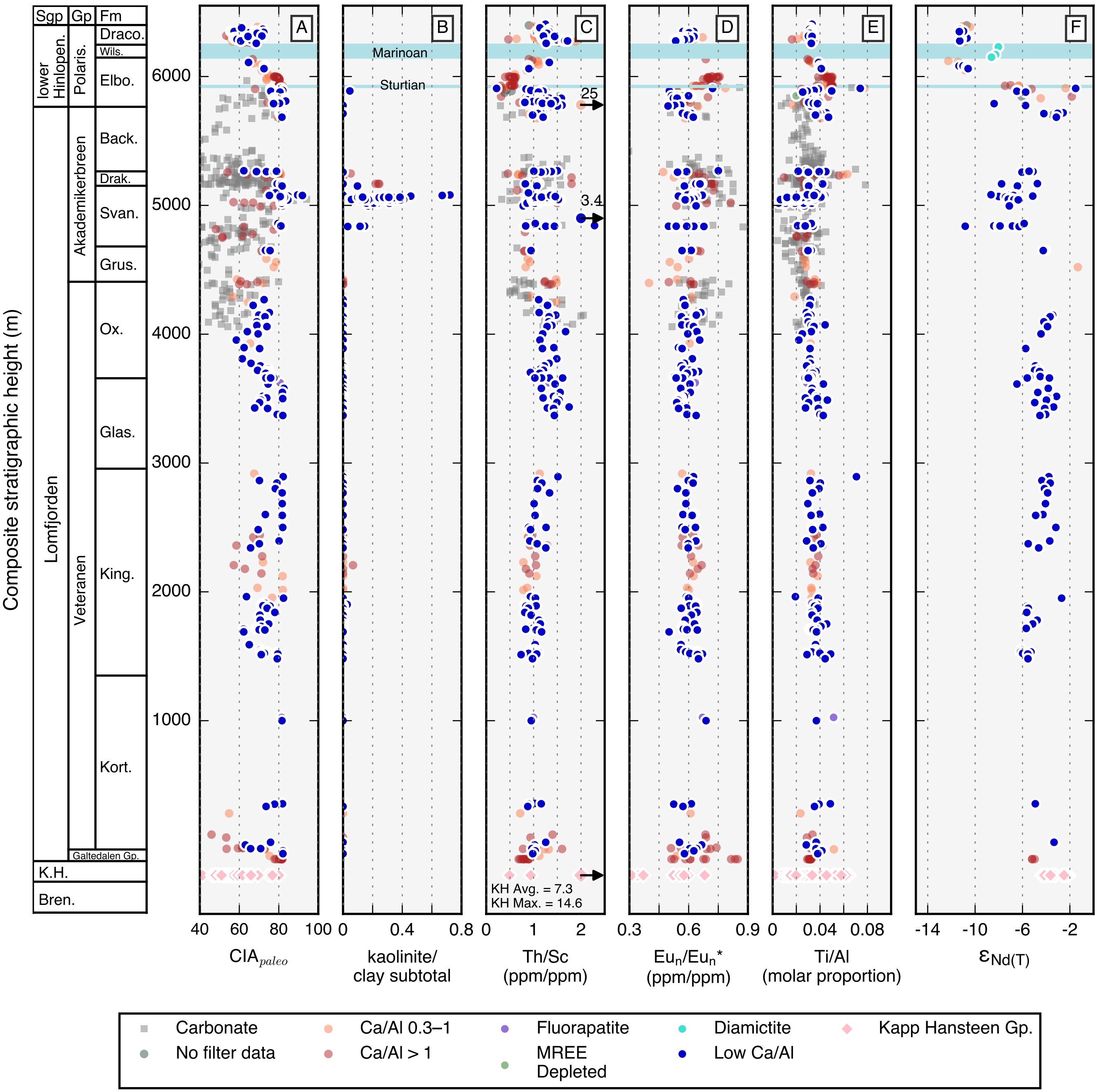

Millikin, Figure 7

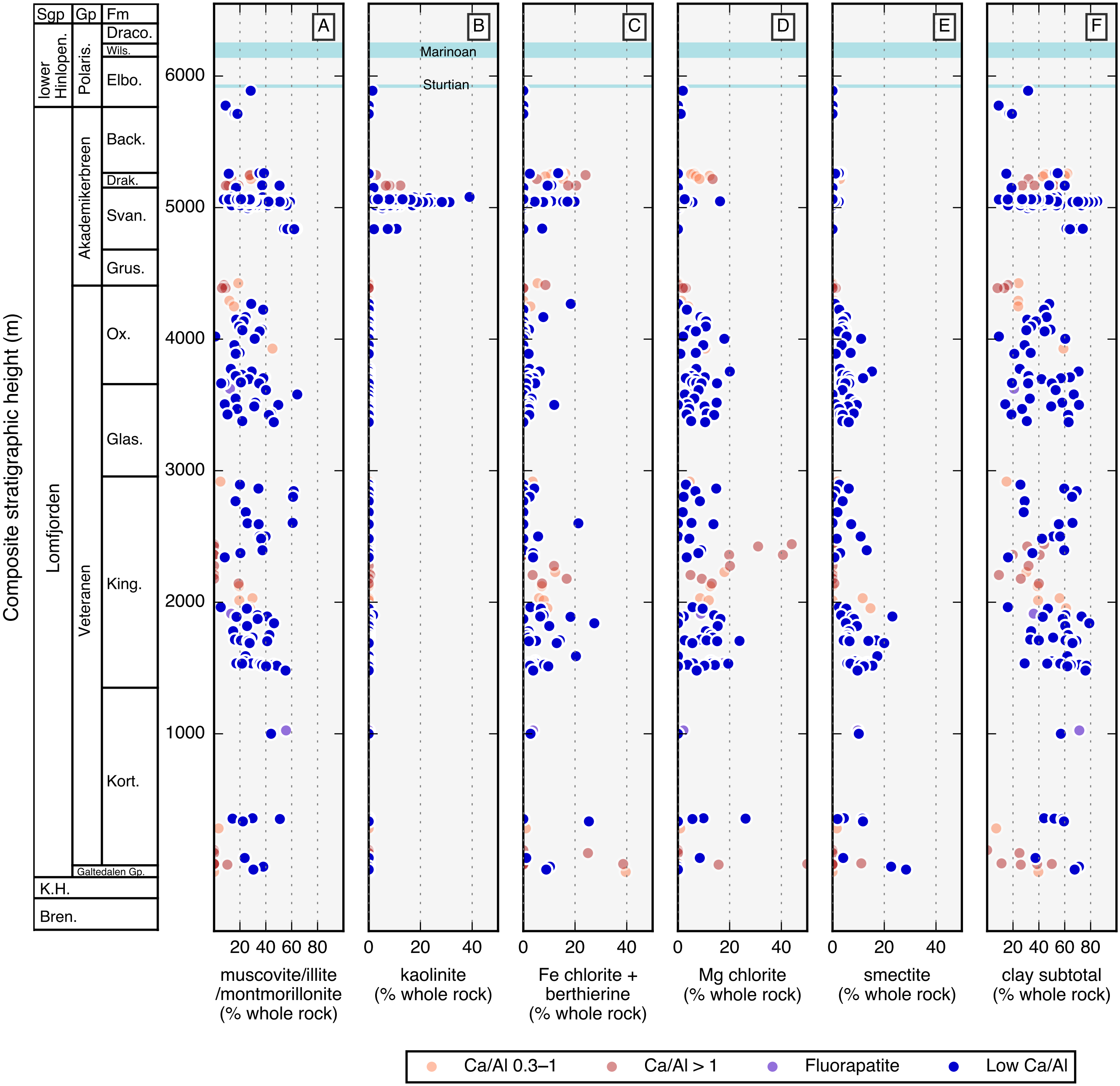

Millikin, Figure DR8

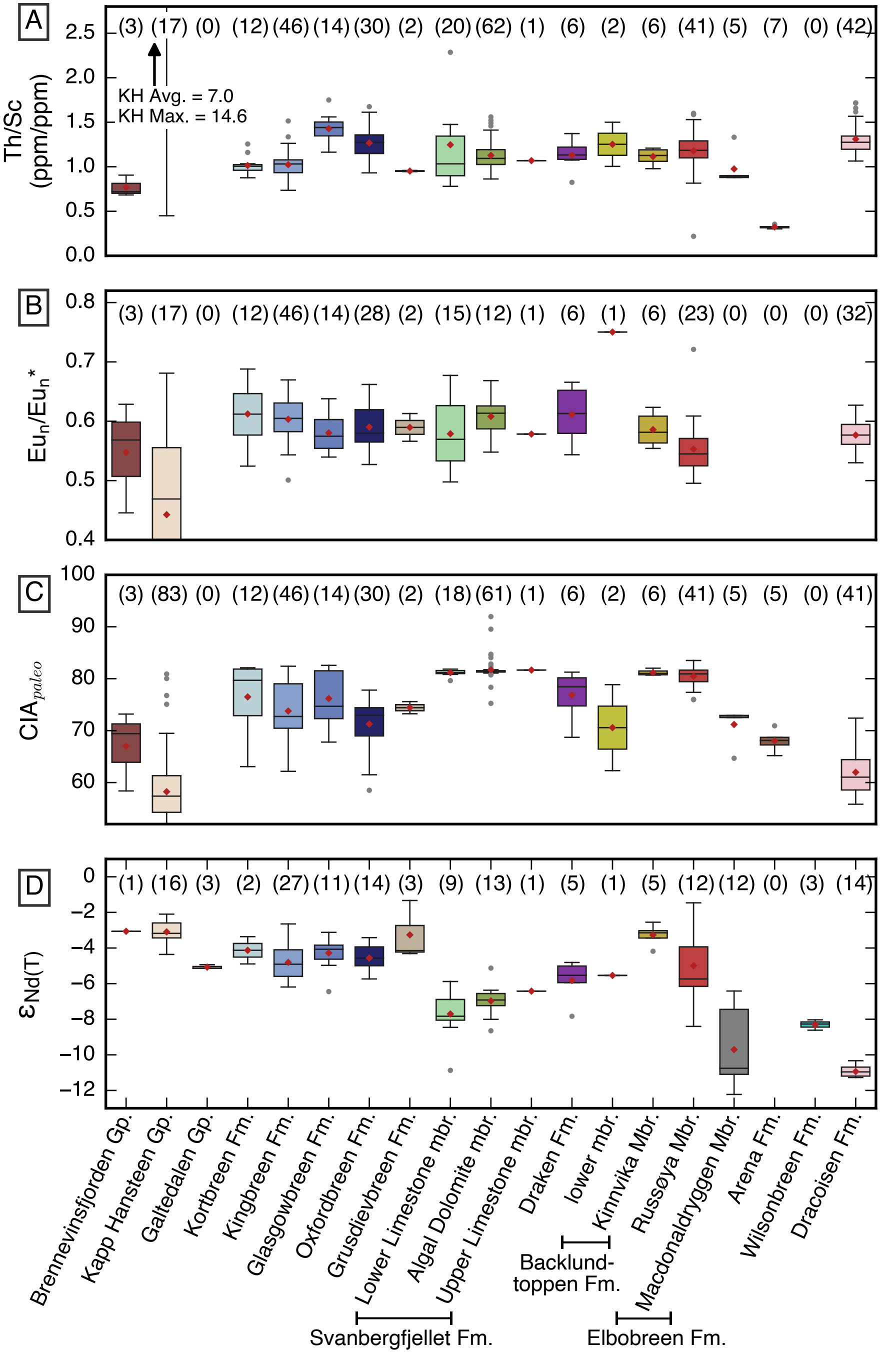

Millikin, Figure 9

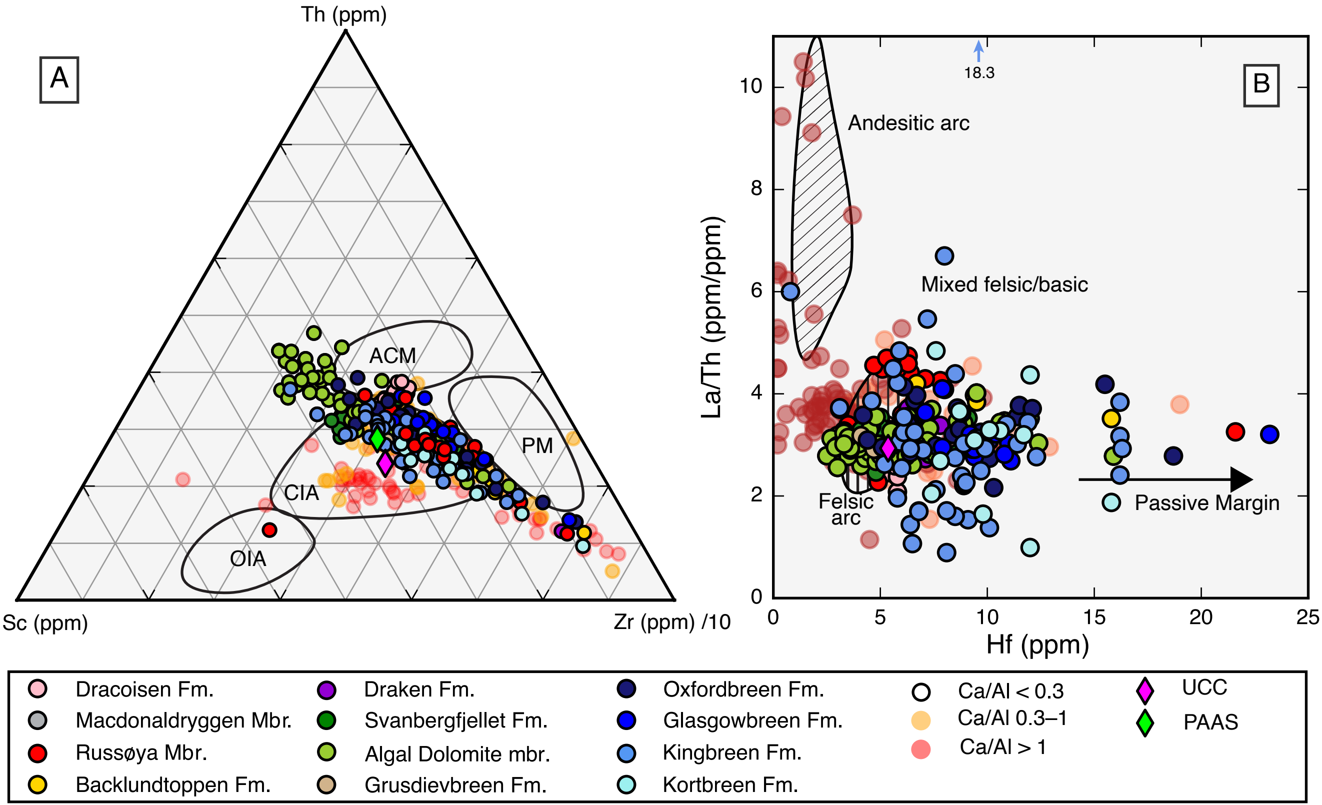

Millikin, Figure 10

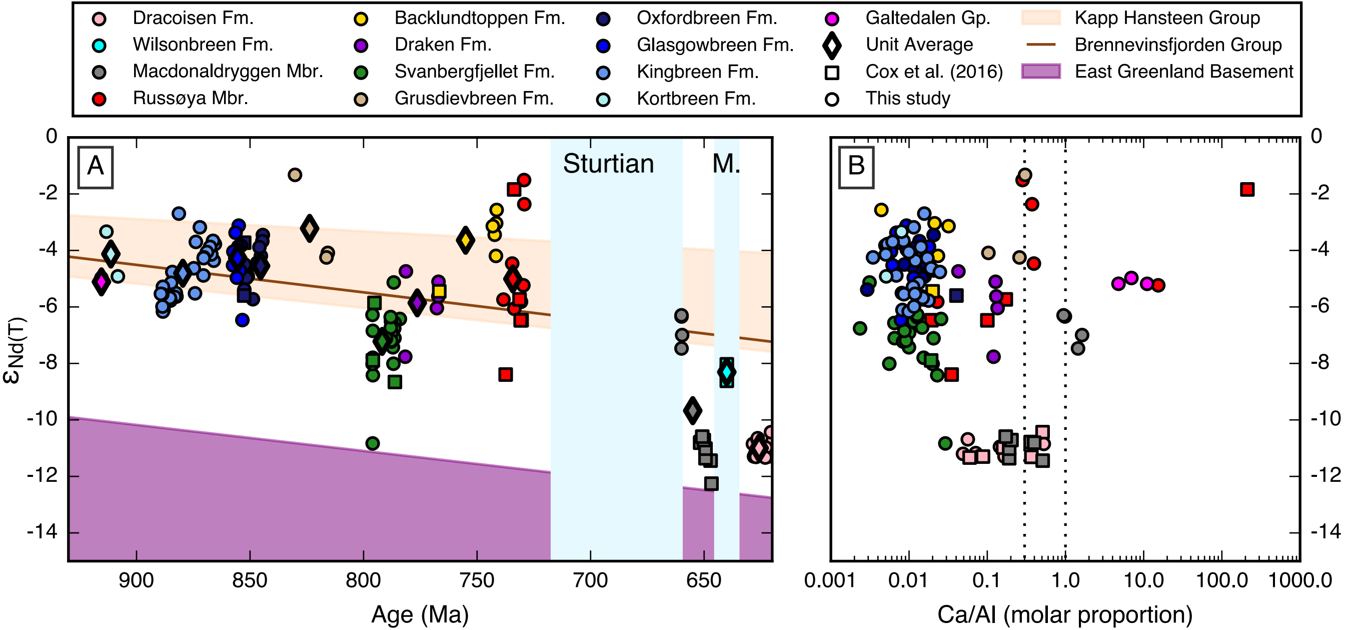

Millikin, Figure 11

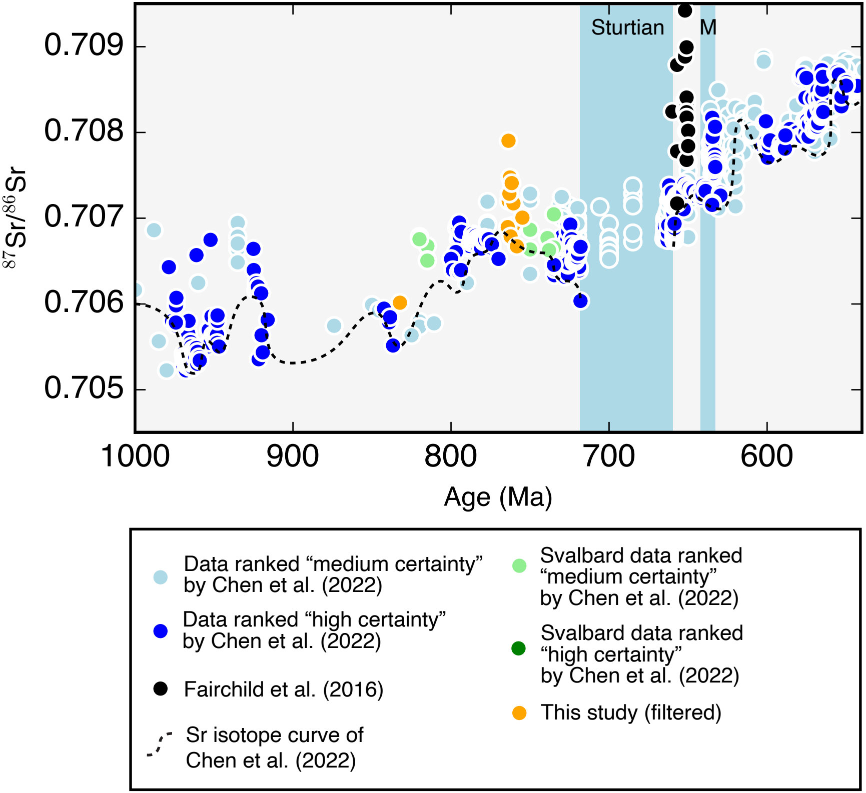

Millikin, Figure 12

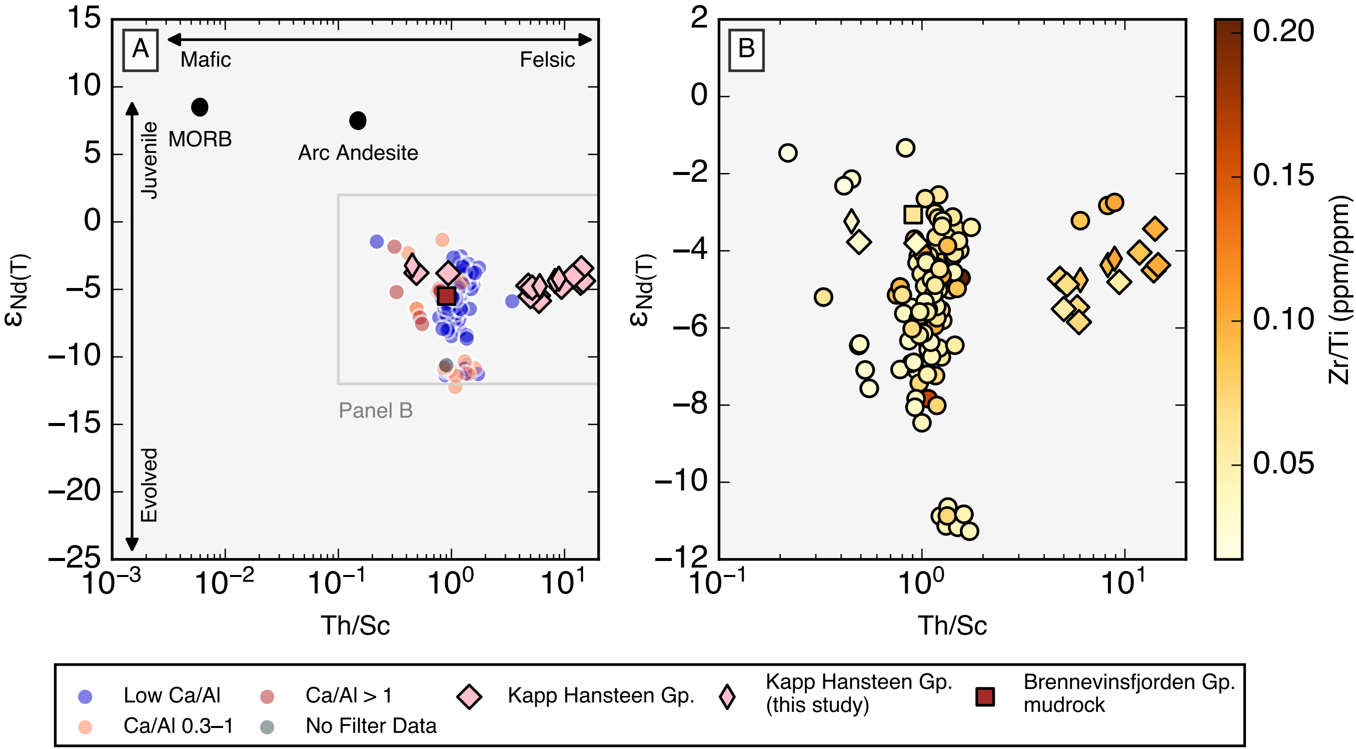

Millikin, Figure 13

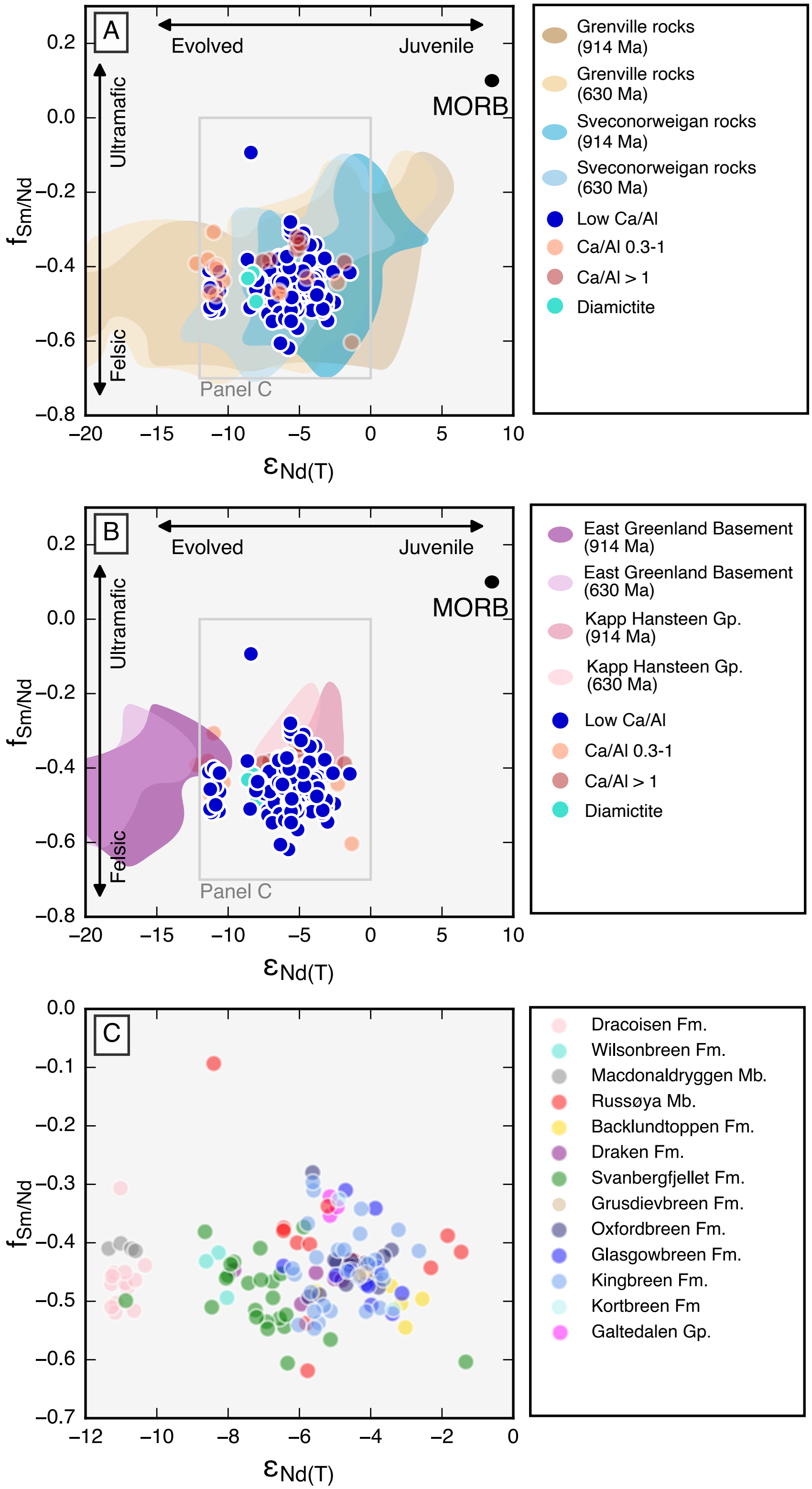

Millikin, Figure 14

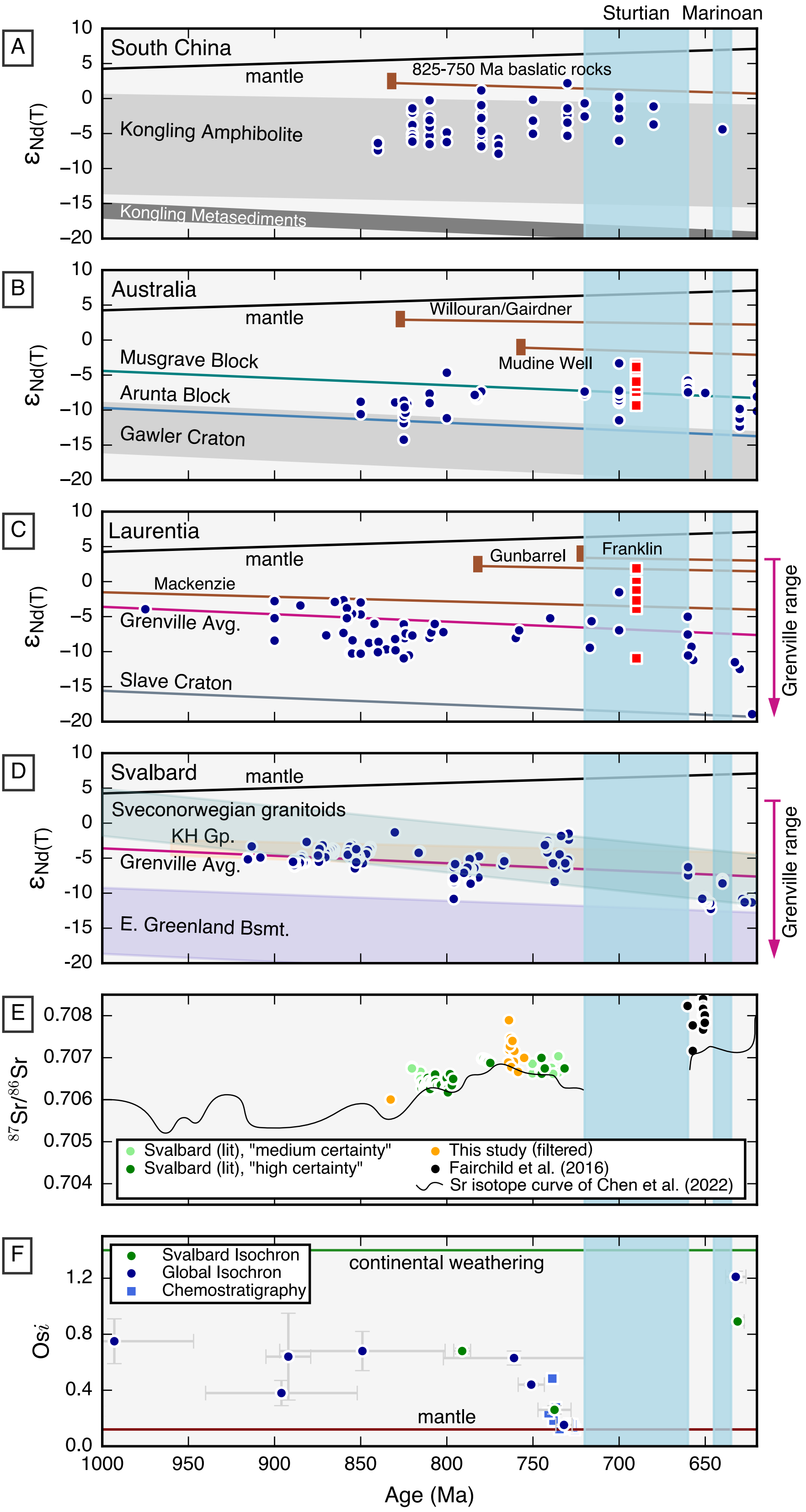

Millikin, Figure 15

TABLE 1. SAMPLE SUBSETS OF THE LOMFJORDEN AND LOWER HINLOPENSTRETET SUPERGROUP SEDIMENTARY ROCKS AND BASEMENT UNITS OF THE BRENNEVINSFJORDEN AND KAPP HANSTEEN GROUPS USED TO FILTER GEOCHEMICAL DATA

Subset Name	Defining characteristics*†	Part of "provenance and weathering subset"#	Lithology	Number of samples
Low Ca/Al	Mudrock with Ca/Al ratio below 0.3 and no significant MREE enrichments or depletions compared to PAAS§	yes	mudrock	287
Fluorapatite	Mudrock with MREE enrichment that is interpreted to reflect heavy mineral enrichment	yes	mudrock	4
MREE Depleted	Mudrock with MREE depletion that is interpreted to reflect weathering or diagenesis of P-bearing minerals	yes	mudrock	11
No filter data	Mudrock without adequate data to filter into other subsets	no	mudrock	8
Ca/Al 0.3–1	Mudrock with Ca/Al ratio between 0.3 and 1	no	mudrock	80
Ca/A > 1	Mudrock with Ca/Al ratio greater than 1	no	mudrock	93
Diamictite	Diamictite lithology determined in field	no	diamictite	3
Carbonate	Carbonate lithology determined in field	no	carbonate	1961
Igneous	Igneous lithology determined in field	no	igneous	4

*Ca/Al calculated using elemental molar proportion

†MREE—Middle Rare Earth Element

§PAAS—Post-Archean average shale

#Subset of mudrock samples used to investigate changes in sediment provenance and weathering conditions